Ray-tracing Based Investigations on the Deployment of RISs in Indoor Scenarios

KONG DEXIN AND NAMBALA SWAROOP
MASTER´S THESIS
DEPARTMENT OF ELECTRICAL AND INFORMATION TECHNOLOGY
FACULTY OF ENGINEERING | LTH | LUND UNIVERSITY

LUND UNIVERSITY

SONY

Ray-tracing Based Investigations on the Deployment of RISs in Indoor Scenarios

Kong, Dexin and Nambala, Swaroop

Department of Electrical and Information Technology
Lund University

Supervisor: Fredrik Rusek (SONY)
Erik Bengtsson (SONY)
Xuesong Cai (Lund University)

Examiner: Buon Kiong Lau (Lund University)

June 14, 2023

Printed in Sweden
Tryckeriet i E-huset, Lund

Abstract

Reconfigurable intelligence surface (RIS) is a promising candidate technology for future 6G wireless communication systems. In existing communication systems, the network operators are unable to control the propagation environment, which causes significant limitations on communication performance. RIS aims to create favorable propagation conditions via programmable phase shifts. Employing RIS can improve power/spectrum efficiency, which improves the quality of communication and reduces costs.

Understanding the trade-offs between the number of base stations (BSs) and the number of RISs is highly desired by both industry and academia. To this end, a ray-tracing-based deterministic indoor channel model is developed. Based on the ray tracing simulator, this thesis aims at providing trade-offs between the number of BSs and the number of RISs regarding the received power of user equipment (UE). Ray tracing simulations are made in the Wireless InSite™ software, and data processing in MATLAB™. To investigate the trade-offs, we evaluate the communication performance with different numbers of activated RISs and BSs. Here, our approach is to investigate a large number of tentative deployed BS/RIS positions and constrain the number of activated BS/RIS and the minimum acceptable power threshold at UE. Given the constraints, we optimize over the BS/RIS placements. In total, four optimization problems are solved in this thesis. We will present our mathematical modeling of optimization problems and how we solve them using MATLAB™.

After the completion of the thesis, we conclude that deploying a small number of RISs can reduce the number of BSs in indoor scenarios without any performance loss regarding the received power at UE. Moreover, RIS is more applicable in environments with abundant shadowing objects. Allowing a non-zero outage probability, i.e., dropping some UE positions with bad communication conditions, is verified to improve power efficiency greatly. Lastly, we also show the necessity to optimize the phase shifts of RIS to enhance the RIS performance in a wideband system.

Popular Science Summary

Manipulating natural elements like air and water has been associated with an art called magic. If you are able to control nature by yourself, you are called either a magician or a science fiction character. But what if it was possible to manipulate how electromagnetic waves move in an environment? Maybe not total control but in a way that improves wireless communication from what it is today. This is possible with an emerging technology candidate called reconfigurable intelligent surface (RIS) in the emerging 6G wireless communication standard.

With a RIS, we will be able to control the physical environment to an extent for it to be compared to magic. We have all complained about important calls being cut because the signal quality has dropped or while we are streaming an exciting science fiction series, the video stops and buffers or mobile operators spending ginormous amounts of money to improve service quality. What if using a RIS we are able to mitigate these issues? Advancements in RIS research show improvements in increasing the range of existing systems, increasing energy efficiency and improving system security.

If so, then how many of these promising products, i.e., RIS, might be needed to see a justifiable improvement in wireless communication in a given scenario? To answer this question, we would need a procedure to find out how to perform this evaluation, mathematical proof backing this method, data-driven results to validate the claims made earlier, and a defined measure of justifiable improvement. Our master thesis on "Ray-tracing Based Investigations on the Deployment of RISs in Indoor Scenarios" answers these questions and opens doors to many other possibilities in using this potentially groundbreaking technology. We encourage the readers to go through our thesis report to understand how we have answered the aforementioned questions using mathematics and simulations with an interesting technique called Ray-tracing.

Acknowledgement

First, We would like to express our great appreciation to our supervisors Dr. Fredrik Rusek, Dr. Erik Bengtsson at SONY, and Dr. Xuesong Cai at Lund University, for their critical guidance and patience. We want to thank all our colleagues in the R&D department at SONY. Working at SONY for the last six months has been a great pleasure. We are touched by their patience and kindness very much.

Then we also want to express our deep gratitude to all the employees at the Department of Electrical and Information Technology, Lund University. It is an invaluable journey to study wireless communication in this department. Your education grants us the key to our future careers.

Dexin Kong and Swaroop Nambala

A personal acknowledgment from Swaroop Nambala: I want to be thankful to my life partner Ms. Divya Prathyusha Malla, for offering immense support and keeping my spirits up during this time. You have been an instrumental strength in my life and have always encouraged me. I am eternally grateful for that.

Swaroop Nambala

A personal acknowledgment from Dexin Kong: I want to express my deep gratitude to my dear parents, Mr. Lingjian Kong and Mrs. Lei Zhou, for supporting and encouraging me all the time. Their love is my greatest motivation to become a good person. With their love, I am able to overcome all the challenges. I am also grateful for the continuous help from my dear friends Chun Xu, Yuanqing Fu, and Zonghan Wang. Working with them for the last two years has been my pleasure!

Dexin Kong

Table of Contents

List of Figures

List of Tables

List of Acronyms

3D	Three Dimensional
5G	Fifth-Generation Mobile System Standard
6G	Sixth-Generation Mobile System Standard
AWGN	Additive White Gaussian Noise
BS	Base Station
CIR	Channel Impulse Response
DL	Downlink
EM	Electromagnetic
GPS	Global Positioning System
GPU	Graphics Processing Unit
I.I.D	Independent and Identically Distributed
JCAS	Joint Communication and Sensing
LOS	Line-of-Sight
MILP	Mixted Integer Linear Programming
MIMO	Multiple-Input Multiple-Output System

MISO	Multiple-Input Single-Output System
mmWave	Millimeter Wave
PDP	Power Delay Profile
QoS	Quality of Service
RF	Radio Frequency
RIS	Reconfigurable Intelligent Surface
SIMO	Single-Input Multiple-Output System
SNR	Signal-to-Noise Ratio
THz	Tera-Hertz
UE	User Equipment
UL	Uplink

Chapter 1
Introduction

In this chapter, we put forth the motivation for this thesis project. As for the background information, we provide some details on ray tracing, which is the channel modeling method employed in this project. We then introduce some emerging technology candidates for 6G.

1.1 Motivation

From the first generation to the fifth generation, communication systems have empowered countless new technologies and shaped modern society in many positive aspects. With data traffic rocketing, improving the spectrum efficiency of existing systems and utilizing new spectrums are critical. Towards sixth-generation (6G) communication, millimeter wave (mmWave) and Tera-Hertz (THz) channels have attracted great attention because of their abundant spectrum resource [1]-[3]. However, with increased center frequencies, electromagnetic (EM) waves' propagation properties deteriorate, resulting in less diffraction, scattering, and penetration. Even a wooden desk can cause blockage. Although some existing communication technologies, such as massive multiple-input multiple-output (MIMO) or distributed MIMO, can combat bad channel conditions, energy/cost efficiency is a significant challenge. Moreover, with increased operating frequency, the coverage of each base station (BS) decreases, which leads to dense network deployment. The inter-cell interference will limit the performance of the communication system unless complex interference cancellation schemes are applied. In [4] and [5], the authors envision distributed architectures, such as distributed MIMO, as the future of communication system architecture. However, deploying many access points/BSs is very challenging for network operators.

Considering the hardware cost and energy consumption, reconfigurable intelligent surface (RIS) is a promising candidate technology in 6G to improve spectrum efficiency and coverage [6]. The research in [7]-[9] envisions that RIS is able to accommodate the impairments of the channel via programmable phase shifts and amplitudes. Instead of only staying in the comfort zone of conventional communication systems, integrating the RISs with other solutions, such as distributed architectures, is a promising research direction regarding system performance and cost. To the best of the authors' knowledge, the trade-off between cost and system performance has never been studied despite the abundant research on RIS

configuration and implementation.

1.2 Project Goals

When discussing RIS technology, a few questions arise, such as how many elements are enough in a RIS? How much can a RIS improve the system performance? How many RISs are needed in an indoor scenario? Does an added RIS allow for the removal of some BSs? These questions still remain largely unanswered. Our thesis aims to understand how a RIS impacts wireless communication in an indoor scenario and to find the trade-off between the number of deployed BSs and the number of deployed RISs in indoor scenarios. To be more specific, we would like to build an office scenario in the ray tracing software in accordance with the SONY Lund office and perform ray tracing simulations in the sub-6GHz frequency range. We then investigate the system performance with respect to coverage. We present two approaches on how to search for the optimum system performance. Comparing the optimum system performance, we search for the trade-offs between the number of BSs and the number of RISs. Here, we also introduce a passive RIS structure and propose our RIS structure.

1.3 Approach and Methodology

As the title indicates, this project is based on ray tracing simulations using Wireless InSite™ software. According to floorplans of SONY's office in Lund, Sweden, we create a ray tracing model of it. We extract the channel impulse response (CIR) from the output of ray tracing simulations and calculate channel transfer functions in MATLAB™. As for the performance evaluation, we implement two approaches. We deploy a large number of tentative BSs and RISs in feasible positions, which are many more than what is reasonable. Then, we search among those positions for the optimal placements for a given constraint on the number of activated BS/RIS. The first approach is to search exhaustively for the optimum combination of different numbers of active BSs among all subsets concerning the mean received power of user equipment (UE). Then, standard optimization packages in MATLAB™ are employed and benchmarked against exhaustive search (when possible). In this thesis, the built-in function 'intlinprog' is used to solve the mixed integer linear programming (MILP), and the function 'fminunc' is used to solve unconstrained optimization problems.

1.4 Thesis Organization

In Chapter 2, we lay down the background information about new features empowered by RIS in future communication systems, channel modeling, and the application scenario of RISs. In Chapter 3, we give an overview of RIS-assisted communication systems and discuss an example of active RIS structure design. In Chapter 4, we provide the steps of making a ray tracing simulation model in accordance with SONY's office in Lund, Sweden. To find trade-offs mentioned in

the project goals, we search for the optimum combinations under different numbers of active BSs and RISs. In Chapter 5, we solve four optimization problems based on two approaches and draw some conclusions from the optimization results. Chapter 6 discusses RIS performance in a heavily shadowed environment. Lastly, we summarize our work and provide future research directions in Chapter 7.

Chapter 2
Background

In this chapter, we present background information necessary for understanding this thesis. The 6G standard is being shaped to envision a high-fidelity holographic society to provide connectivity for all things and to enable time-sensitive applications [1, 2]. New features such as wireless power transfer [10], joint communication and sensing (JCAS) [11, 12], and positioning [13] will be empowered by future communication systems. Many emerging candidate technologies are available for implementation. In the following sections, we introduce two features for 6G that RIS can empower, namely, Sensing and Positioning. Moreover, we discuss the methodology for obtaining channels as well as the application scenario for RIS deployment.

2.1 Sensing and Positioning Enhanced by RIS

Sensing is one of the key differentiators of future communication systems in comparison to existing communication systems [11]. Nowadays, positioning is widely used by billions of people worldwide. Web mapping platforms like Google Maps, Apple Maps, and Baidu Maps rely highly on positioning technologies empowered by satellites (GPS). As known, The performance of GPS degrades significantly in indoor environments, but radio-based positioning using 6G could potentially solve this issue. Future 6G communication systems are envisioned for seamless wireless connectivity beyond traditional information transmission [7]. Without consuming more spectrum and power, sensing and positioning can be achieved to obtain more information, such as people's health information, environmental information, the speed of the vehicles, the location of devices, etc. Sensing and positioning are new functions of future communication systems and improve the system's communication performance. Utilizing sensing and positioning to obtain environmental information enables the communication device to enhance channel estimation, resource scheduling, etc. In this thesis, we do not focus on sensing and positioning in detail. Still, if a RIS can improve communication capabilities through better exploitation of the spatial domain, then this would also have positive implications for sensing and positioning. It is envisioned that a RIS can compensate for bad communication conditions in [8, 9, 14], thus, enhancing the accuracy of sensing and positioning.

2.2 Methodology for Obtaining Channels

To investigate RIS performance, we need different channel models to study it. There are different alternatives to how these channel models can be developed. Channel sounding is widely used to measure the real channel, and the properties of the measured channel can be extracted to develop a channel model. Ray tracing is another approach to obtaining a deterministic channel model, which is employed in this thesis. Here, we provide some information about these two alternatives and compare them.

2.2.1 Channel Sounding

Moving higher up the frequency bands available for communication, the significance of understanding the medium of propagation or "channel" is increasing prominently. Now that we are commercially deploying 5G networks worldwide, the dependence on channel knowledge is quite significant. The wireless channel is essentially the medium through which radio waves propagate. Intuitively, the transmitter and receiver locations are essential for determining some information about the channel. Channel sounding is a technique where we transmit a signal, known on both the transmitter and receiver side, in the environment of interest and observe how this signal has changed on the receiver side. The changes of interest might vary from a wide array of available channel parameters like delay spread, Doppler spread, etc. The structure of the channel sounder and the type of sounding signal used varies with the required parameter of interest. The extracted channel properties from the measurement results are then utilized to develop channel models.

2.2.2 Ray Tracing

Treating EM waves as rays has been explained in detail in [15]. The ray concept makes it convinient to visualize propagation within an environment and is the basis underlying ray tracing. The idea behind ray tracing is to use mathematical computations to understand the changes undergone in the channel and map them on a visualization environment, preferably a three-dimensional one, for visual comprehension. In other words, it can be loosely described as following a wave, characterized as a ray, and marking its movement in the propagation environment. Even though the idea is quite intuitive, the application, however, becomes quite complicated when the calculations are done by a human. A computer, however, might be capable of performing multiple calculations if it has the processing power to do so. Recent advancements in the evolution of graphics processing units (GPUs) have made it possible to perform these calculations on a computer in a practically feasible time frame. There are a few aspects of wireless channels where ray tracing calculations do not agree with real-time measurements, but received power has been shown to differ less than 5dB in [16].

2.3 Why Ray Tracing or Ray Tracing vs. Channel Sounding

The primary aim of our thesis is to understand how significantly RISs impact wireless communication in an indoor environment. Our approach is to select proper performance metrics and compare the performance with or without RISs present, perform an analysis, and draw conclusions from the results. First, we need a channel model to perform some calculations for any environment. It is essential to mention that we are referring to a deterministic channel model in the previous statement. The aforementioned model can be obtained by measuring the channel using a channel sounder or by building a 3D model of the environment and performing ray tracing. Although channel sounder gives an accurate channel model compared to its counterpart, access to one is quite difficult because of monetary and availability reasons. Moreover, moving objects physically when using a channel sounder is often required to change the environment and re-run the experiment. These limitations present ray tracing as an alternative solution to channel sounding. Ray tracing is much more convenient for changing the environment as it is a computer model, and objects can be moved around with a few clicks on the mouse. It is not fair to say that ray tracing is always better than channel sounding, but for our conditions, it is preferable. Now that we have established why we have chosen to move forward with ray tracing, we would like to discuss the RIS structure further and how we define our implementation.

2.4 Application Scenario

The idea of utilizing a RIS is to solve the coverage problem. We place all transmit antennas in a BS in the existing communication system. By deploying a large number of highly-directive antennas, perhaps small-scale fading can be accommodated. However, large-scale fading caused by the shadowing of large objects, e.g., walls and windows, can not be compensated (see Figure 2.1). The received signals are very weak for the UEs located in the edge zone of a cell, and the inter-cell interference is considerable (see Figure 2.2). In Figure 2.1 and Figure 2.2, all light green dots are the UE positions, all the rays are the propagation paths between one BS and one UE position, and the ray color shows the power level of each path (orange indicates a weak signal). In Figure 2.1, the BS (deep green dot) serves one unlucky UE position shadowed by the walls. In Figure 2.2, the BS (red isotropic antenna) serves one UE position located in the edge zone.

How can we improve the quality of service (QoS) under these conditions? BS units are extremely expensive, and we cannot keep adding BSs for these unlucky UEs. Besides, dense BS deployment will introduce more inter-cell interference, which may degrade the system performance. RIS can be a perfect solution for future communication systems. Figure 2.3 and Figure 2.4 illustrate how a RIS can be deployed to improve the QoS, where one RIS is employed in each scenario. In Figure 2.3, one RIS is employed in the corner to collect the signals originating from the BS and forward the signals to the UE. In Figure 2.4, one RIS is employed near the UE to provide a large array gain which enhances the signals forwarded to the UE in the edge zone.

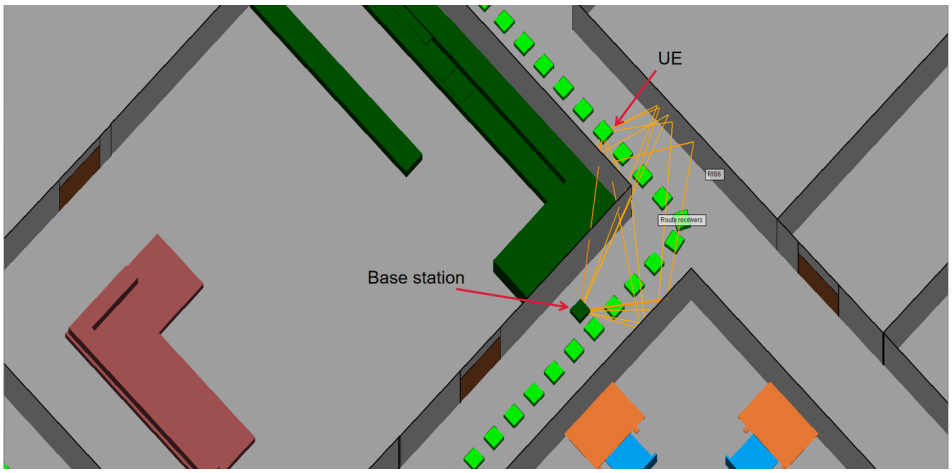

Figure 2.1: Shadowed UE position

Figure 2.2: Edge UE position

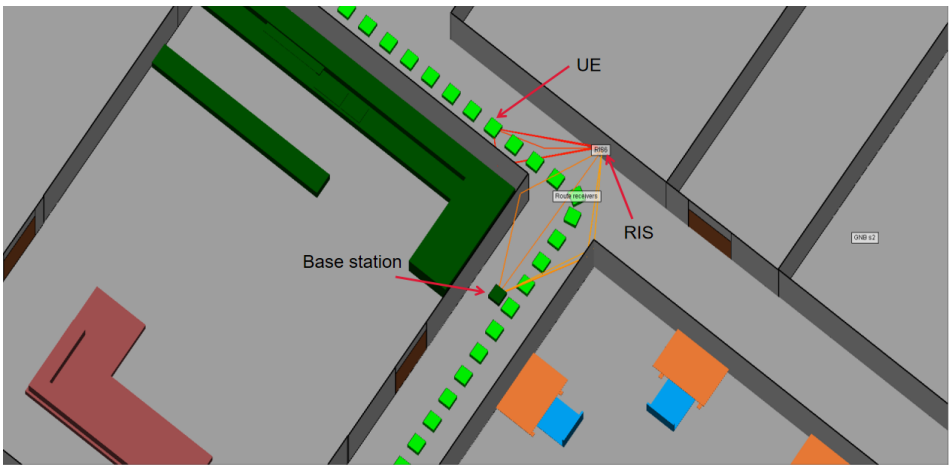

Figure 2.3: RIS-assisted communication for Shadowed UE position

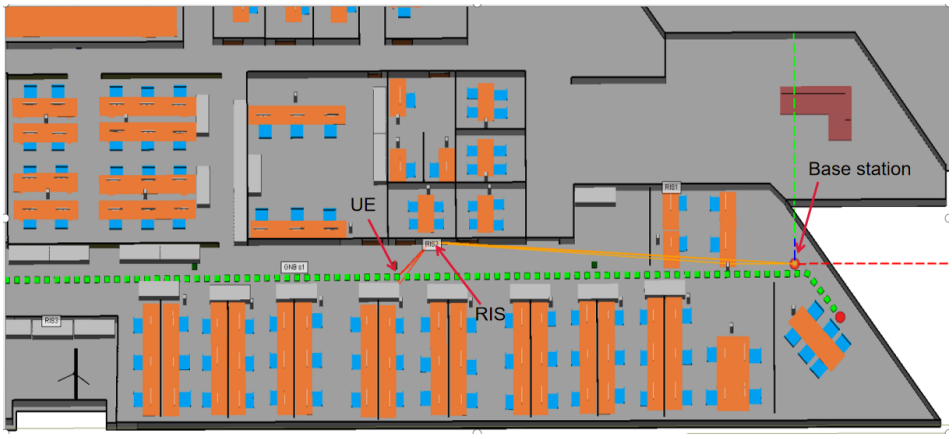

Figure 2.4: RIS-assisted communication for Edge UE position

Chapter 3
Reconfigurable Intelligent Surface

As mentioned in the previous section, RIS is a promising candidate technology for future communication systems. Chapter 3 discusses the RIS definition, structure, and implementation. We also present one important law: the quadratic signal-to-noise ratio (SNR) gain law of RIS.

3.1 What is a RIS?

RIS is a thin surface comprising a massive number of low-cost elements which are sub-wavelength distributed. A RIS typically has a large aperture resulting in a high array gain. With a high array gain, RIS-assisted communication links can enhance the received signal at the UE. Additionally, proper beamforming is required at the RIS [9]. Therefore, each element of a RIS is connected to a phase shifter. RIS can control the propagation environment by programmable phase shifts. It is noteworthy that our work assumes the optimal phase shifts of the RIS but is not dealing with how these phase shifts are obtained. At this time, we have numerous ways to define a RIS or how to implement it. Loosely speaking, a RIS is a planar surface made of metamaterials or antenna elements to direct signal propagation in desired directions without any involvement from baseband components. RISs are deployed as wall mounts in desirable locations. By utilizing RISs, we can improve coverage and reduce interference without consuming more power.

3.2 RIS-assisted Communication Channel

The wireless communication channel of a RIS-assisted communication system is called the cascaded fading channel because the signals in the RIS-assisted communication link undergo the channel fading twice, that is, the link from the BS to the RIS and the link from the RIS to the UE.

According to the Friis transmission, stated in Equation 3.1, the received power at an antenna element of a UE can be calculated using the transmitted power, antenna efficiency, wavelength, and propagation distance. Assuming P_{t} is the transmitted power from the BS, and P_{UE} is the received power at the UE. G_{T}, G_{RIS}, and G_{UE} are all antenna efficiencies. The propagation distance from the BS to the RIS is denoted by d_1, and the propagation distance from the RIS to the UE

is denoted by d_2. The wavelength of the propagation signal is λ. As a result, the received power of the UE is calculated by Equation 3.2.

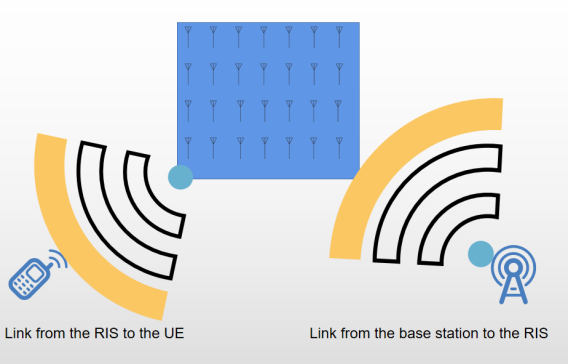

Figure 3.1: RIS-assisted communication Channel

$$P_{\mathrm{r}} = P_{\mathrm{t}} G_{\mathrm{t}} G_{\mathrm{r}} \left(\frac{\lambda}{4\pi d} \right)^2 \tag{3.1}$$

$$P_{\mathrm{UE}} = P_{\mathrm{t}} G_{\mathrm{t}} G_{\mathrm{RIS}} G_{\mathrm{UE}} \left(\frac{\lambda}{4\pi d_1} \right)^2 \left(\frac{\lambda}{4\pi d_2} \right)^2 \tag{3.2}$$

In general, there are two types of RIS: active and passive RIS implementations which are studied later. The most significant difference between an active RIS to a passive RIS is that a power amplifier (gain) is added to an active RIS. In the following sections, we discuss passive RIS implementations and how our implementation differs from this.

3.3 Passive RIS Structure

One popular RIS structure is the passive RIS structure shown in Figure 3.2. One advantage of a passive RIS is that all elements should be nearly passive, which means no radio frequency (RF) chain inside the RIS [17, 18]. As a result, passive RIS is a promising technology to improve power/cost efficiencies. From Figure 3.2, we can observe that each antenna is connected to one phase shifter, which is used to compensate for the phase shifts of the cascaded fading channel. The signal at each antenna is phase-shifted before being reflected back at the termination and then leaving from the very same antenna.

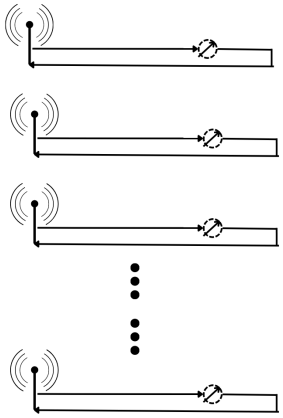

Figure 3.2: Passive RIS structure

3.4 Active RIS Structure

There are multiple different approaches to implementing an active RIS [19]. Figure 3.3 shows the implementation of an active RIS. Different from the passive RIS structure, we have more components present in the RIS. The RIS has two sides, one targeting the UE and one targeting the BS. Although physically, the antennas on both sides may or may not be the same, we have separated them to distinguish the channel between the BS and RIS and the channel between the RIS and UE. There are two sets of phase compensators, one toward the BSs and one toward the UE. The function of a phase compensator is to add phase to the input signal. This phase can be positive and negative and tuned according to our requirements. We also have a power combiner, a power amplifier, and a power splitter present in this RIS. The intention behind these components shall be explained later.

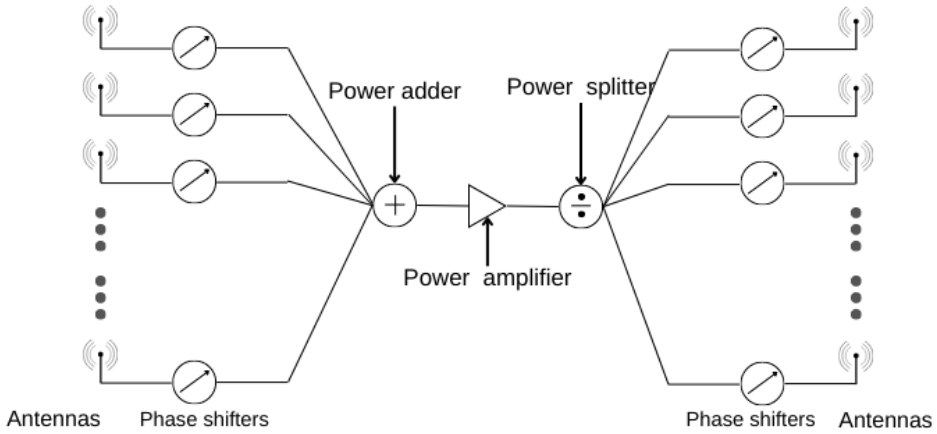

Figure 3.3: Structure of our RIS

The structure presented in Figure 3.3 is unidirectional, i.e., it can only serve either Uplink (UL) or Downlink (DL). If bi-directional transmissions are needed, then one may proceed according to one of the following bullet points:

- Use a bi-directional amplifier, which requires a special design.
- Reconfigure the RIS
- Use two identical structures next to each other. One for UL and one for DL.

The main objective of this RIS is to add signals from a BS constructively toward a UE location. To achieve this goal, in simpler words, a RIS must collect the signal from the transmitter and deposit it collectively on the receiver side. We can obtain the phase from the channel obtained using the results of ray tracing, which will be explained in more detail in later sections. Using this information in the phase compensators, we can constructively achieve the intended objective and add the signals constructively. The problem of obtaining these phase shifts in an actual system is another question and not studied in this thesis. At this point, it is very important to mention that the phase information we obtain for the channel is for a narrow-band frequency but not a wide-band system. This is because the channel in the simulation environment depends on the frequency or, in other words, a frequency-dependent channel from our observations. Phase compensation for a wideband scenario is discussed in Section 5.4.

3.5 SNR Gain of a RIS

In this section, we provide the derivations of one important law of RIS: the quadratic SNR gain law of RIS.

3.5.1 Parameters

Figure 3.4 refers to a RIS-assisted narrowband communication system where the BS transmits the signal s to the RIS, and the UE collects the signal r via a RIS in between. We assume this RIS has m elements on each side. Let $\boldsymbol{H}_{\mathrm{Tx}}$ denote the channel transfer function from the BS to the RIS and $\boldsymbol{H}_{\mathrm{Rx}}$ denote the channel transfer function from the RIS to the UE (see Equations 3.3a and 3.3b). Equation 3.3c indicates the phase shifts on the left side of the RIS shown in Figure 3.3 and denoted by θ_k. Equation 3.3d indicates the phase shifts on the right side and is denoted by ϕ_k. From Equations 3.3e to 3.3f, $\boldsymbol{V}_1$ and $\boldsymbol{V}_2$ are the beamforming vectors. G is the power amplification factor, $\boldsymbol{N}$ is the noise in the RIS and w is the noise in the receiver. Both $\boldsymbol{N}$ and w absorb several quantities, for example,

path loss.

$$\boldsymbol{H}_{\mathrm{Tx}} = [h_{\mathrm{tx}1}, h_{\mathrm{tx}2}, h_{\mathrm{tx}3}, \cdots, h_{\mathrm{tx}m}]^{\mathrm{T}} \tag{3.3a}$$
$$\boldsymbol{H}_{\mathrm{Rx}} = [[h_{\mathrm{rx}1}, h_{\mathrm{rx}2}, h_{\mathrm{rx}3}, \cdots, h_{\mathrm{rx}m}] \tag{3.3b}$$
$$\boldsymbol{\theta} = [\theta_1, \theta_2, \theta_3, \cdots, \theta_n] \tag{3.3c}$$
$$\boldsymbol{\phi} = [\phi_1, \phi_2, \phi_3, \cdots, \phi_n]^{\mathrm{T}} \tag{3.3d}$$
$$\boldsymbol{V}_1 = \exp(j\boldsymbol{\theta}) \tag{3.3e}$$
$$\boldsymbol{V}_2 = \exp(j\boldsymbol{\phi}) \tag{3.3f}$$
$$\boldsymbol{N} \in \mathcal{CN}(0, N_{01}I) \tag{3.3g}$$
$$w \in \mathcal{CN}(0, N_{02}) \tag{3.3h}$$

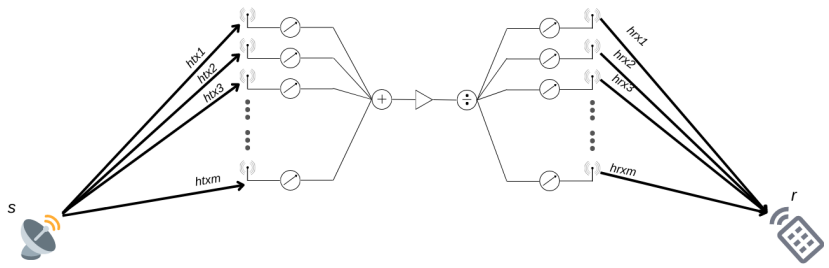

Figure 3.4: RIS-assisted communication system

3.5.2 Signal model

For simplicity, we transmit a signal s with unit average power and an i.i.d Rayleigh channel. Here, we only focus on the power domain. Further, we assume equal large-scale fading across the entire array and power normalization according to the following:

$$\mathbb{E}\{|s|^2\} = 1 \tag{3.4a}$$
$$\mathbb{E}\{|h_{\mathrm{tx}i}|^2\} = 1 \quad i \in \{1, 2, ..., m\} \tag{3.4b}$$
$$\mathbb{E}\{|h_{\mathrm{rx}i}|^2\} = 1 \quad i \in \{1, 2, ..., m\} \tag{3.4c}$$

Therefore, the received signal r and SNR at the UE are shown in Equations 3.5a and 3.5b. One may notice there is one parameter m in the following equations, which is the number of elements in a RIS. The division is due to the effects of a power splitter. Equation 3.5b is the expected SNR. That is a ratio of signal and noise, where we take the expectation of the numerator and denominator individ-

ually.

$$r = \boldsymbol{H}_{\mathrm{Rx}} \boldsymbol{V}_2 \left(\frac{\sqrt{G} \boldsymbol{H}_{\mathrm{Tx}} \boldsymbol{V}_1 s + \sqrt{G} N}{m} \right) + w \tag{3.5a}$$

$$\mathrm{SNR} = \frac{m^2 G}{G m N_{01} + N_{02}} \tag{3.5b}$$

As one can observe from Equation 3.5b, the SNR gain is quadratic in the number of elements m in a RIS. Notably, if GmN_{01} is much larger than N_{02}, the validity of this quadratic SNR law vanishes. It is because GmN_{01} will be attenuated by the cascaded fading channel.

3.6 Advantages of Active RIS Structure

When discussing the passive RIS structure in the above section, we mentioned that one advantage of RIS is energy efficiency. However, passive beamforming is often not significant enough to compensate for the cascaded fading channel. Due to the nature of the cascaded fading channel, the placement possibility of a RIS is very limited. Generally speaking, every RIS should be placed very close to a BS or a UE [9]. However, the network operator can only have a limited number of positions to place a RIS or BS (see Figure 3.5).

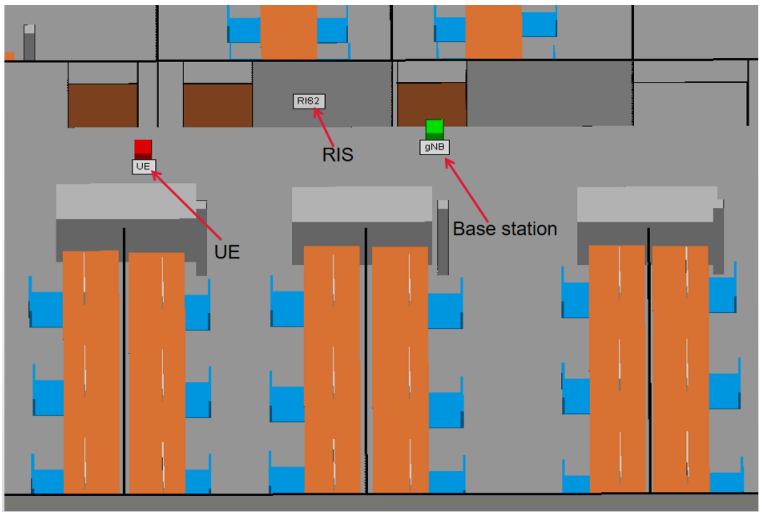

Figure 3.5: Practical scenario

If we put a RIS midway between a BS and a UE, the cascaded fading channel will make the RIS-assisted communication link nearly useless. To overcome this challenge, we choose to add a power amplifier. An active RIS, shown in Figure 3.3, can buy us more flexibility, which means we can put a RIS in any position. Another noteworthy point is that our RIS has two facing sides instead of one facing side for a passive RIS. It means that our RIS has more application scenarios than the

passive RIS. Figure 3.5 shows a case of RIS deployment where a RIS lies midway between the UE and the BS. Here, the passive RIS cannot compensate for the cascaded fading channel, stated in Equation 3.2, while an active RIS can.

Chapter 4
Ray Tracing Simulations

In the following sections, we discuss Wireless InSite™, the software used in ray tracing, and explain in detail how we designed the simulation environment, any shortcomings or compromises we made, and justifications for them.

4.1 Ray Tracing Using Wireless InSite™

We have established that we need to have channel information to make an analysis or conclude on observations. We have also established that we can obtain the above-mentioned channel information using ray tracing. To perform ray tracing using Wireless InSite™, we must decide on a simulation environment. This environment must have a logical or scientific justification for our conclusions and results to be valid and significant. The environment must be indoors as we investigate RIS performance in indoor scenarios. This requirement leads to potential candidates such as shopping malls, office buildings, hospitals, etc. We moved forward with an office building as we have some perspective and resources to build this environment immediately. The third floor of the SONY office building was chosen as the simulation environment, as we have a floor plan with detailed dimensions available. This environment has the authenticity of a real office building, and many objects contribute to a realistic channel seen in indoor deployment scenarios. An office floor usually consists of cupboards, doors, windows, partitions, computers, tables, and chairs. But we also have unique cylindrical cable towers, which significantly influences the channel and must be included in the simulation environment.

All the aforementioned objects were modeled in 3D using a licensed 3D modeling tool known as 3Ds Max. The dimensions of every object present on the third floor of Sony were measured using the laser-guided scale to ensure accuracy. We had to photograph multiple office areas to understand how to place the objects within the environment in Wireless InSite™. The environment post positioning of aforementioned objects looks as in Figures 4.1 and 4.2. Figure 4.1 shows a long green dotted line passing throughout the environment. This is the trajectory of the user, traveling from one end of the office to the other end. Figure 4.2 shows the same simulation environment with 16 BSs, placed as a grid, covering the entire environment without the UE trajectory. There are other entities within Figure 4.1, which shall be explained later. Although objects like wires and stationary

are present physically, we could ignore them as they are electrically smaller than the wavelength of signals within the environment. The following section describes which antennas we will be using, how we have constructed the RISs in the environment, and where to place the BSs.

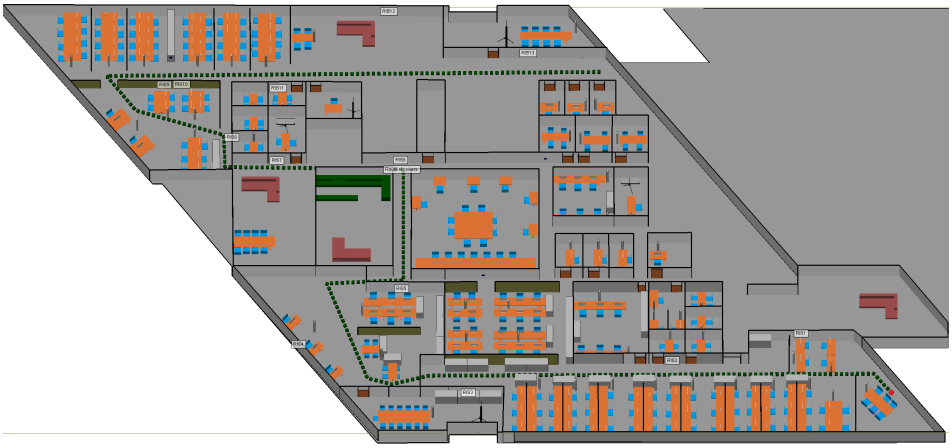

Figure 4.1: Simulation environment - only UE (Rx) shown in the Figure

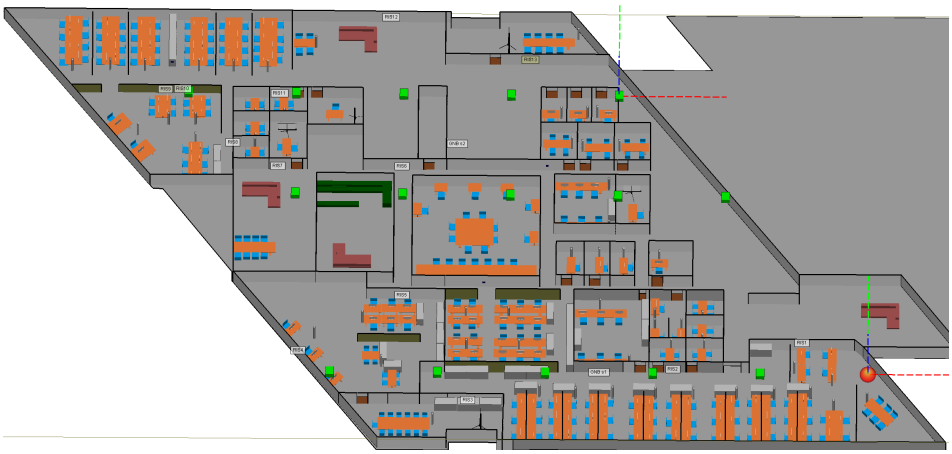

Figure 4.2: Simulation environment - only BSs (Tx) shown in the Figure

4.2 Antenna Configuration

This section discusses the simulator configuration to produce the relevant results for developing a channel model. The software requires antenna patterns as input

to apply them to any antenna element within the environment, either a Tx (BS), RIS, or Rx (UE). These patterns can be chosen from pre-existing options, or the UE can be designed independently. The choice of radiation pattern has a significant impact on the outputs from the software, as we have observed in our numerous trials. When rectangular patch antennas were used, in some test cases, it was observed that line-of-sight (LOS) paths were weaker in received power than reflection and diffraction paths by a significant amount. One may think that this goes against widely established theory and common sense because LOS has the least propagation loss. We have found out that this is due to the directivity and radiation pattern of the patch antenna is not uniform at every angle. If a LOS path is coming from an angle where the directivity is weaker and a reflected path at an angle with more directivity, the aforementioned phenomenon happens. As the goal of the thesis is not to investigate radiation patterns in the RIS, we have chosen to use an isotropic radiation pattern in our simulation environment for the RIS. Similarly, to prevent any further obvious errors such as the one mentioned earlier, we decided to move forward with isotropic antennas in the BSs as well as the UEs. A 9-element RIS looks, in the software, as in Figure 4.3.

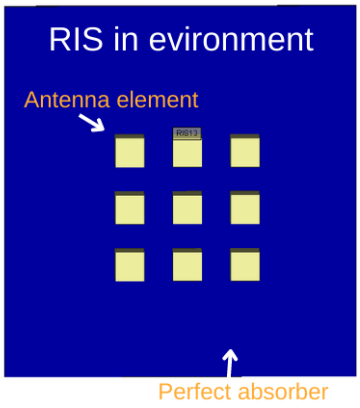

Figure 4.3: RIS configuration

Each cuboid is an antenna element with an isotropic radiation pattern. This radiation pattern can be observed in the lower left corner. A perfect absorber was placed behind every RIS, which can be seen as the blue area sheet in Figure 4.3. This was done to prevent antenna elements from picking up paths coming from behind the RIS. We would not need a perfect absorber if the antenna elements have non-isotropic patterns. But as explained in the previous paragraph, that introduces issues discussed in the previous sentences, issues we would definitely

like to avoid. The perfect absorber absorbs all paths falling on its surface and will not allow them to be registered on the antenna elements.

4.3 BS and RIS Placement

As mentioned earlier, the green dots that can be observed in Figure 4.1 indicate the path of a UE moving within the environment. The UE position was 1.8m above ground, considering a human's average height. It is our intention to move the UE from one end of the environment to the other end and observe how the channel varies from one position to the other and identify the basis for the chosen trajectory. We have observed from simulations, as well as from derivations, that having a RIS in the middle between a BS and a UE location will not yield good results in terms of performance. It would be beneficial to have a RIS closer to the UE or the BSs [8, 9].

Turning to the BSs, ideally, it would be perfect to have the BSs on the ceiling spread out in a grid in the entire environment. This way, we would know which location in the grid is best for placing BSs. Achieving this requires the program to calculate the propagation paths for every one of these grid points individually to every other green point in the path shown in Figure 4.3. It is our belief that placing BSs at every grid point and calculating ray tracing data has an overwhelming complexity and is not feasible to carry out with the hardware we have. We have also verified this by actually using a grid of 27 BSs to evaluate this computation problem, and the program crashed after 3 days of run time. It is also important to note that this calculation has not yet included the presence of a RIS in the environment, which might complicate the calculation time to a greater extent. As mentioned earlier, having a RIS closer to a UE or closer to a BS has better performance in received power compared to having it in the middle of the path. Using this metric, we have placed RISs along the path of the UE on the adjacent walls wherever possible. It is important to note that the positions of BSs and RISs are tentative, and we wish to choose the best possible locations in the later sections.

Up to this point, we have provided an overview of calculating a channel based on ray tracing, the principle for employing this technique, an approach to implementing a RIS, the simulation environment design, and BS/RIS placement methodology. After finishing all these steps, we are ready to run a simulation and obtain the required results. In the following section, we would like to explain the output of a ray tracing simulation and how we calculate a channel realization from it.

4.4 Channel Model or Calculating the Channel Model or Channel between Tx-Rx or Channel between BS-UE

Wireless InSite™ software allows UEs to choose what outputs to display and store among many available parameters. We obtained the CIR using every path from a transmitter to a receiver. These files contain how many paths exist from a Tx to

Rx, the delay at which each path arrives, the phase at the Rx location, and the power received. It is important to note that when we refer here to transmitter and receiver, we mean a transmitter and receiver in general, not the BS and UE. Using this information, we can calculate the channel transfer function ($H(f)$) within our environment by taking the Fourier transform of the calculated CIR. It is explained in detail in the following paragraph.

Equation 4.1 is the basis for obtaining complex impulse responses from the data mentioned in the previous paragraph.

$$h(\tau) = \sum_{k=1}^{K} a_k \delta(\tau - \tau_k) \exp(j\theta_k) \tag{4.1}$$

Here K is the total number of paths between the transmitter and receiver, $\delta(t)$ the Dirac-delta function in t, and θ_k the phase of the incoming signal. If we assumed $h(\tau)$ to be the impulse response between a transmitter and a receiver, then the channel transfer function would be $H(f)$. This calculation can be done by taking a Fourier transform of the complex impulse response.

$$H(f) = \int_0^{\infty} h(\tau) \exp(-j2\pi f\tau) \mathrm{d}\tau \tag{4.2}$$

Equation 4.2 can be rewritten as Equation 4.3 when we have substituted Equation 4.1.

$$H(f) = \int_0^{\infty} \sum_{k=1}^{K} a_k \delta(\tau - \tau_k) \exp(j\theta_k) \exp(-j2\pi f\tau) \mathrm{d}\tau \tag{4.3}$$

Upon rearrangement of the integral and summation terms within Equation 4.3, we arrive at Equation 4.4.

$$H(f) = \sum_{k=1}^{K} a_k \exp(j\theta_k) \exp(-j2\pi f\tau_k) \tag{4.4}$$

The property $\int_0^{\infty} \delta(t - t_k) f(t) \mathrm{d}t = f(t_k)$ of the Dirac-delta function was used to move from Equation 4.3 to Equation 4.4. Figure 4.4 is a plot of the channel transfer function of the channel calculated using Equations 4.1 - 4.4.

4.5 Channel between BS-RIS-UE

The channel between the BS and UE, or the direct link, was calculated as described in the previous section. After running the simulation, relevant parameters to calculate CIR were extracted from the output files of Wireless InSite™. A Fourier transform of this CIR resulted in the channel transfer function. The magnitude squared of the channel transfer function, also called the channel gain, was computed. But obtaining the channel between BS-RIS-UE or RIS-assisted link is slightly different from what was described in the previous section.

We view the channel as the cascading of two separate channels, one between the BS and RIS and one between the RIS and UE. If we were to assume the

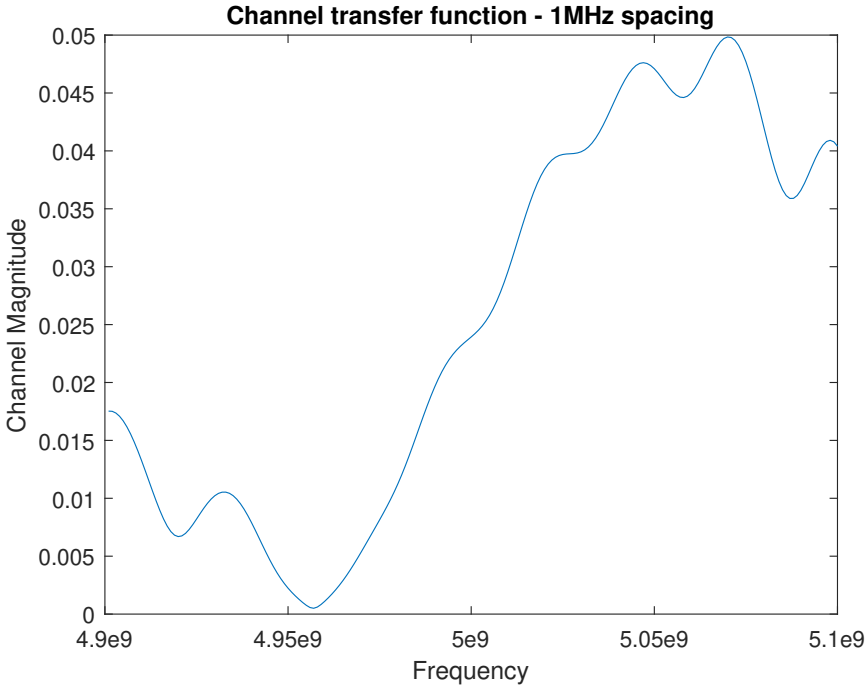

Figure 4.4: Channel transfer function for frequency range from 4.9GHz to 5.1GHz

narrowband channel transfer function vector between BS and RIS to be $\boldsymbol{H}_{\mathrm{Tx}}$ and the narrowband channel transfer function vector between RIS and UE to be $\boldsymbol{H}_{\mathrm{Rx}}$, then cascading makes the entire channel look like $\boldsymbol{H}_{\mathrm{Tx}}\boldsymbol{H}_{\mathrm{Rx}}$. It is important to note that at this moment, $\boldsymbol{H}_{\mathrm{Tx}}$ and $\boldsymbol{H}_{\mathrm{Rx}}$ do not contain the phase compensation as mentioned in Section 3.5.1.

4.5.1 Narrowband case

Referring to Section 2.2, we have phase compensation present in the RIS, which must be included in the calculation. When the channel between the BSs and RIS is considered, the system is modeled as a single-input multiple-output (SIMO) system for a single frequency, and the channel between UE and RIS is modeled as a multiple-input single-output (MISO) system. For the SIMO part, the channel vector is given in Equation 4.5

$$\boldsymbol{H}_{\mathrm{Tx}} = \begin{bmatrix} h_{\mathrm{tx1}} & h_{\mathrm{tx2}} & \cdots & h_{\mathrm{tx}m} \end{bmatrix}^{\mathrm{T}} \tag{4.5}$$

and MISO part, the channel matrix is given in Equation 4.6

$$\boldsymbol{H}_{\mathrm{Rx}} = \begin{bmatrix} h_{\mathrm{rx1}} & h_{\mathrm{rx2}} & \cdots & h_{\mathrm{rx}m} \end{bmatrix} \tag{4.6}$$

Equation 4.7 gives the cascaded channel with phase compensation.

$$H_{\text{BS-RIS-UE}} = \frac{\sum_{i=1}^{m} h_{\text{tx}i}\exp(j\theta_i)\sqrt{G}}{m} \sum_{i=1}^{m} h_{\text{rx}i}\exp(j\phi_i) \tag{4.7}$$

where θ_i and ϕ_i are the phase compensation toward Tx and Rx sides, respectively. The m in Equation 4.7 is a factor arising from the power splitter in Figure 3.3. In this section, Tx and Rx refer to the BS and UE, respectively.

4.5.2 Wideband case

For a wideband system, the channel becomes a matrix instead of a vector, and we observed the presence of frequency selectivity in Figure 4.4. The channel between the BS and RIS looks as in Equation 4.8.

$$\boldsymbol{H}_{\text{Tx-WB}} = \begin{bmatrix} h_{\text{tx1f}_1} & \cdots & h_{\text{tx1f}_c} & \cdots & h_{\text{tx1f}_P} \\ h_{\text{tx2f}_1} & \cdots & h_{\text{tx2f}_c} & \cdots & h_{\text{tx2f}_P} \\ \vdots & \vdots & \vdots & \vdots & \vdots \\ h_{\text{tx}m\text{f}_1} & \cdots & h_{\text{tx}m\text{f}_c} & \cdots & h_{\text{tx}m\text{f}_P} \end{bmatrix} \tag{4.8}$$

$\boldsymbol{H}_{\text{Tx-WB}}$ is an $m \times P$ matrix, where m is the number of elements present in a RIS and P is the number of frequency samples present in the bandwidth under consideration. Similarly, the channel between RIS and UE looks as in Equation 4.9

$$\boldsymbol{H}_{\text{Rx-WB}} = \begin{bmatrix} h_{\text{rx1f}_1} & h_{\text{rx2f}_1} & \cdots & h_{\text{rx}m\text{f}_1} \\ \vdots & \vdots & \vdots & \vdots \\ h_{\text{rx1f}_c} & h_{\text{rx2f}_c} & \cdots & h_{\text{rx}m\text{f}_c} \\ \vdots & \vdots & \vdots & \vdots \\ h_{\text{rx1f}_P} & h_{\text{rx2f}_P} & \cdots & h_{\text{rx}m\text{f}_P} \end{bmatrix} \tag{4.9}$$

As mentioned in Sub-section 2.7.1, ideally, we would like θ_i and ϕ_i to be the negative angles of $h_{\text{tx}i}$ and $h_{\text{rx}i}$. In other words, we want $h_{\text{tx}i} = \exp(-j\theta_i)$ and $h_{\text{rx}i} = \exp(-j\phi_i)$. But in a wideband system, $h_{\text{tx}i\text{f}_j}$, $h_{\text{rx}i\text{f}_j}$ and $h_{\text{tx}i\text{f}_k}$, $h_{\text{rx}i\text{f}_k}$ may be different unless $j = k$. This presented a complication in formulating the channel matrix of the entire system as a RIS can only take one value of θ_i and ϕ_i in Equation 4.7. So choosing which phase compensation is also a question we had to solve, and until now, we have applied θ_i and ϕ_i calculated at the center frequency f_c for all frequencies of interest. Finding the optimum phases for θ_i and ϕ_i will be discussed in later sections of this report.

Chapter 5

Optimization

So far, we have discussed the goals of our project in Chapter 1. We provided some background information on different aspects related to the project and potential use cases in Chapter 2. Then we gave a comprehensive outline about RIS and its implementation in Chapter 3. In Chapter 4, we discussed information related to ray tracing simulations and their outputs and provided background on how we obtained the relevant channel parameters in the narrowband and wideband scenarios. In this chapter, we will focus on optimizing our communication system. As mentioned before, the primary goal of this project was to find trade-offs between different selections of BSs and RISs for deployment.

Looking back to our ray tracing simulation result, we deployed 16 BSs and 13 RISs to serve 315 UE positions, the points on the green trajectory of Figure 4.1. In this Chapter, we provide two approaches to finding the optimum performance. To be more detailed, we deploy a set of cleverly chosen tentative positions. Then, some constraints are given on the number of activated BSs and RISs, as well as the power threshold. We start with the simple approach to exhaustively search over these sets to find the optimal subset of activated BSs and RISs serving every position in the UE trajectory, for example, in a scenario where we may only need to activate 5 BSs because of a lack of budget or other considerations. We activate a different subset of 5 BSs every time until we go through all subsets. The second approach is to make use of some standard optimization packages in MATLAB™ to solve this optimization problem. Achieving the optimum performance for the system is a challenging combinatorial optimization problem because many variables have to be considered. To arrive at a solution, it is critical to model the problem as a MILP optimization problem. The following sections will describe, in great detail, four optimization problems with unique targets under consideration. The following subsections refer to a term called "communication link". We use this term to signify an end-to-end link between a transmitter node and a receiver node, possibly via a RIS node. This communication link can be a RIS-assisted or a direct link, and their names imply the presence of a RIS in serving the UE position. In this thesis, we assume there is no cooperation between different BSs/RISs. As a result, the UE is only served by one communication link at every UE position.

5.1 Optimization for BS Selection and Direct Link Selection

To simplify our idea systematically, we planned to observe the performance without any RIS deployed in our environment, where only some BSs serve all UE positions. This selection will also provide a reference for conclusions we might arrive at in subsequent sections. Firstly, we exhaustively searched for the optimal subsets of activated BSs. Secondly, we modeled this problem as a MILP optimization problem to find out which BSs to activate from the preset locations in Figure 4.1 while maximizing the average received power over every UE position. In other words, the optimization problem is to find the optimum subset of BSs as well as the optimum link selection at every UE position to maximize mean received power with a constraint on the power threshold, i.e., the minimum received power at the UE in Figure 4.1.

5.1.1 Exhaustive Search

The objective is to decide where to optimally deploy a limited set of BSs. Based on the results from the ray tracing simulations, we obtained the power in every possible direct link. For example, if we activated 5 BSs every time, the UE always has 5 communication links to the back-end, i.e., 5 activated BSs. At every UE position, the UE selects the direct link with the highest power level. Notably, UE is only served by one direct link at any position. This is by no means necessary nor optimal, but it is what we have chosen. Studying the case of joint detection at all BSs is another problem not studied here. Following this scheme, we can calculate the received power at every UE position.

It is noteworthy that the result of an exhaustive search is always optimum. However, we cannot always employ this approach due to the computation complexity when the number of nodes grows large. Equation 5.1 gives the computation complexity of an exhaustive search.

$$\binom{B}{k} = \frac{B!}{k!(B-k)!} \tag{5.1}$$

where k is here the number of activated BSs, and B is the total number of deployed BSs. For example, $B = 16, k = 5$, i.e., 16 choose 5 = 4368, and this is the complexity for the worst case. The sum of (B, k) is $(2^B)-1$, which is the complexity of searching all subsets of all sizes.

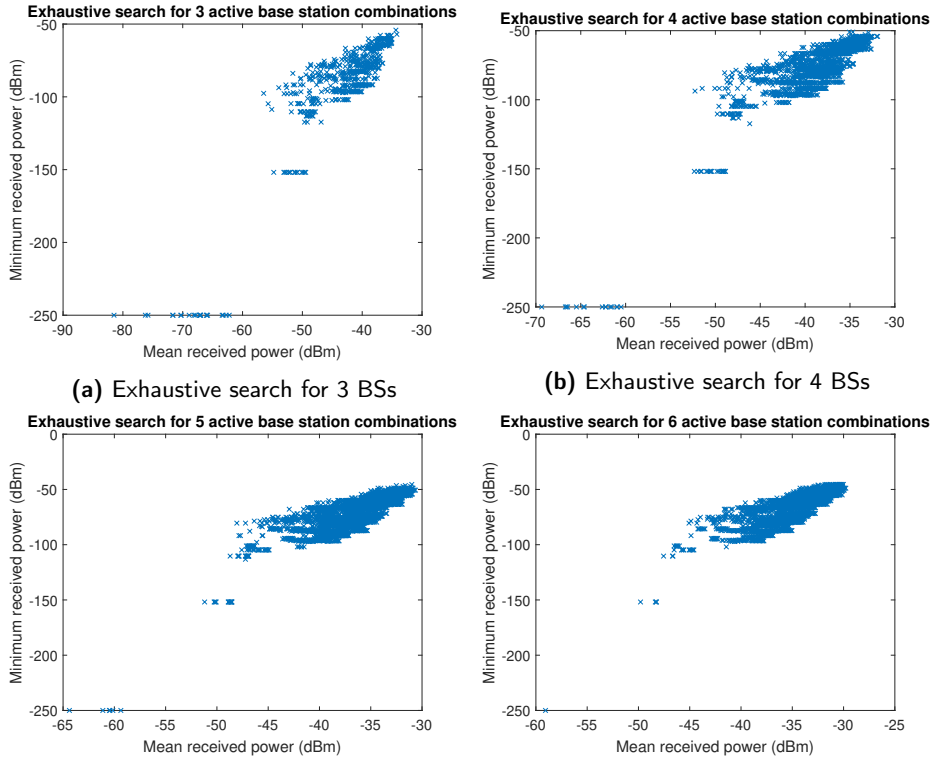

(a) Exhaustive search for 3 BSs

(b) Exhaustive search for 4 BSs

(c) Exhaustive search for 5 BSs

(d) Exhaustive search for 6 BSs

Figure 5.1: Exhaustive search results

Here we provide some results based on the exhaustive search. We searched for all subsets of a number of activated BSs and calculated the mean and minimum received power along the green trajectory. We transmitted the signals with 30 dBm input power from each BS and obtained the ray tracing results. After data processing, the results are shown in Figure 5.1. From Figure 5.1a to Figure 5.1d, the values in the x-axis represent the mean received power, the values in the y-axis represent the minimum received power, and each dot represents the performance of one subset of BSs along the full trajectory. We can observe that the results of the exhaustive search look like clouds. Now, the problem of analyzing the optimum performance of the deployed communication system remains unanswered. How to find the optimum performance based on these clouds?

First, we would like to point out that we have two criteria for evaluating the system performance: mean and minimum received power among all UE positions. It indicates more than one possible optimum solution. Now, we focus on the edge zone of these cloud-looked results, which is in the top-right corner of each plot. In the edge zone, one can observe a Pareto boundary, which is all points that can be considered optimal in Figure 5.2. More figures are attached in the Appendix (Figure A.1 to Figure A.3).

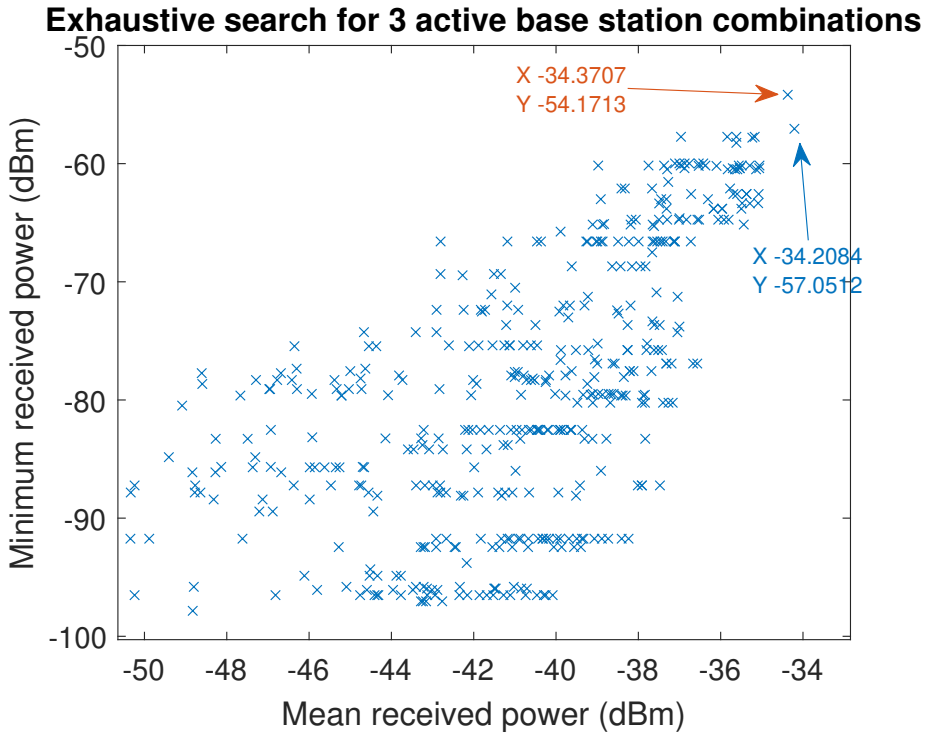

Figure 5.2: Exhaustive search for optimum subsets of 3 BSs

We can find multiple optimum solutions in the edge zones of these cloud-looked results. As shown in Figure 5.2, we can obtain two optimum solutions. One optimum solution has a mean received power of -34.2084 dBm and a minimum received power of -57.0512 dBm. The other optimum solution has a mean received power of -34.3703 dBm and a minimum received power of -54.1713 dBm. It is important to point out that both solutions are optimum. Here, we select both optimum solutions and one non-optimum solution and analyze their quality of service (QoS), which is represented by the received power at every UE position. In Figure 5.3, the values in the x-axis represent the UE position along the green trajectory, and the values in the y-axis represent the received power obtained from the best direct link at each UE position. The blue curve refers to the QoS of the maximum mean received power solution, the red curve refers to the QoS of the maximum minimum received power solution, and the yellow curve refers to the QoS of one non-optimum solution. In Figure 5.3, we call these solutions modes.

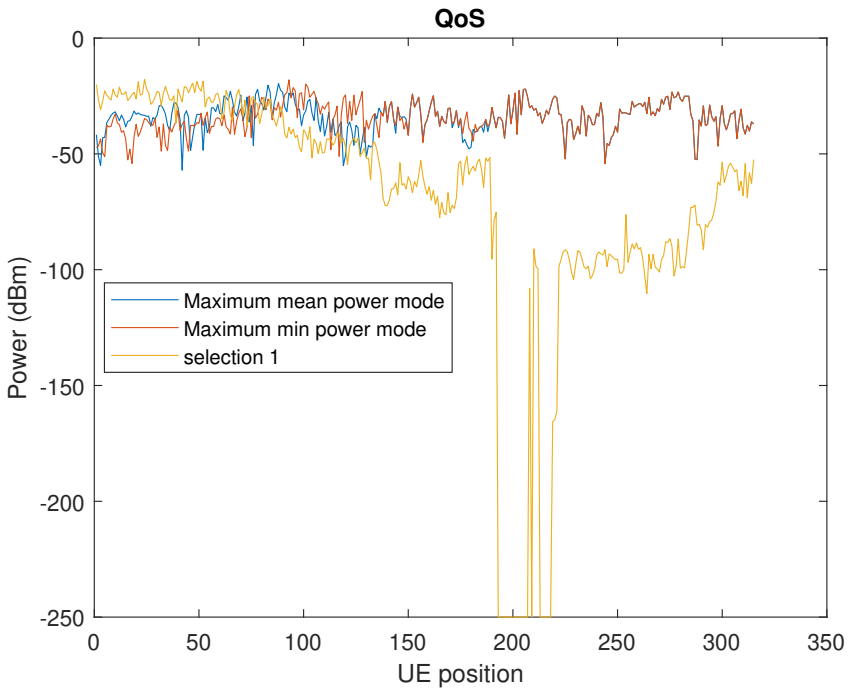

Figure 5.3: QoS comparison

We can draw some conclusions here:

- Optimum solutions cannot ensure every UE position can obtain maximum received power.
- The optimum solutions we search for are to exploit the optimum performance of the full trajectory.
- The received power at an individual UE position might be better than the optimum mode, but the overall system performance is significantly worse than the optimum modes.
- Exhaustive search, by definition, contains all optimum solutions within its subset.
- The complexity of exhaustive search may be a bottleneck when the RISs are added.

5.1.2 Mathematical Model of Optimization

To investigate the optimum selection of direct links, we modeled this problem as a MILP, which can, e.g., be implemented using MATLAB™'s built-in function 'intlinprog.' We also have a few constraints within the problem. In communication systems, a lower limit on received power has been accounted into the optimization problem as a Threshold constraint given by Equation 5.3f. Moreover, we wish to

compare performance for different selections, which means we have a limit on how many BSs are turned "on" We formulate this by saying we only have k active BSs while evaluating performance. The optimization problem, along with the constraints mentioned above, can be seen in Equations 5.2, 5.3a - 5.3f.

$$\max_{q_b, G_{\text{act}}(n,b)} \sum_{b=1}^{B} \sum_{n=1}^{U} P(n,b) G_{\text{act}}(n,b) \tag{5.2}$$

$$\text{subject to } G_{\text{act}}(n,b) \in \{0,1\} \tag{5.3a}$$

$$q_b \in \{0,1\} \tag{5.3b}$$

$$\sum_{b=1}^{B} G_{\text{act}}(n,b) = 1 \quad \forall n \tag{5.3c}$$

$$\sum_{n=1}^{U} G_{\text{act}}(n,b) \leq q_b U \quad \forall b \tag{5.3d}$$

$$\sum_{b=1}^{B} q_b = k \tag{5.3e}$$

$$\sum_{n=1}^{U} G_{\text{act}}(n,b) P(n,b) \geq T \tag{5.3f}$$

Equation 5.2 is the optimization target, which indicates that the primary goal is to maximize the mean received power. $G_{\text{act}}(n,b)$ is a state indicator of the communication link between nth UE position and the bth BS, in which 1 means on and 0 means off. The total number of active BSs and UE positions are denoted by B and U. We use $P(n,b)$ as the received power of nth UE position from the bth BS. This is obtained from the results of ray tracing simulations. Additionally, q_b is the state indicator of the BS b and follows the same notation of 1 and 0 as $G_{\text{act}}(n,b)$. From Equation 5.3c to Equation 5.3d, they constrain that every UE position can only be served by one communication link. Equation 5.3e indicates that the total number of activated BSs is k. Lastly, we set the power threshold in Equation 5.3f.

5.1.3 MATLAB™ Implementation of Optimization

As mentioned in Section 4.4, we obtain a matrix containing the channel gain. We use a transmit power of 30 dBm or 0 dBW, allowing us to simplify the received power at UE position as the channel gain, calculated using methodology explained in Section 4.4. We formulated it into matrix form with the received power from each BS as rows and columns indicating the index of the UE position in the path in Figure 4.1. The UE positions and BSs in the simulated channel are indexed sequentially. The power in each direct link is represented as $P(n,b)$, where each UE position is indexed as n, and the BS is indexed by b. We have verified that all output files have the same number of UE positions to ensure our implementation

was correct. The direct link power can be expanded to a matrix form $\boldsymbol{P}$ as follows.

$$\boldsymbol{P} = \begin{bmatrix} P(1,1) & P(1,2) & \cdots & P(1,U-1) & P(1,U) \\ P(2,1) & P(2,2) & \cdots & P(2,U-1) & P(2,U) \\ \vdots & \vdots & \ddots & \vdots & \vdots \\ P(B-1,1) & P(B-1,2) & \cdots & P(B-1,U-1) & P(B-1,U) \\ P(B,1) & P(B,2) & \cdots & P(B,U-1) & P(B,U) \end{bmatrix}$$

We aim to find an optimized selection of the direct links such that the mean received power is maximized when we choose to activate L BSs from all available combinations. As mentioned in the previous section, we can search for an optimal solution using MILP. The general definition of a MILP problem is given in Equation 5.4.

$$\min_{\boldsymbol{x}} \ \boldsymbol{f}^T\boldsymbol{x} \text{ subject to } \begin{cases} \mathcal{I} = \{i : x_i \in \mathbb{Z}\} \text{ (The indices of integer values in } \boldsymbol{x}) \\ \boldsymbol{A}_{\text{ineq}}\boldsymbol{x} \leq \boldsymbol{b}_{\text{ineq}} \\ \boldsymbol{A}_{\text{eq}}\boldsymbol{x} = \boldsymbol{b}_{\text{eq}} \\ \boldsymbol{l} \leq \boldsymbol{x} \leq \boldsymbol{u} \end{cases} \tag{5.4}$$

where the notation $\boldsymbol{A}\boldsymbol{x} \leq \boldsymbol{b}$ specifies the inequalities $\boldsymbol{a}_\ell\boldsymbol{x} \leq b_\ell$, $\forall \ell$, where $\boldsymbol{a}_\ell$ is the ℓth row of $\boldsymbol{A}$, etc. The intlinprog function of MATLAB™ needs the following inputs.

- The column vector $\boldsymbol{f}$ over which the minimization occurs
- the indices of integer cells in the vector $\boldsymbol{x}$.
- The inequality conditions $\boldsymbol{A}_{\text{ineq}}$ and $\boldsymbol{b}_{\text{ineq}}$
- The equality conditions $\boldsymbol{A}_{\text{eq}}$ and $\boldsymbol{b}_{\text{eq}}$
- Upper and lower bounds $\boldsymbol{l}$ and $\boldsymbol{u}$

It is important to observe that the solver in MATLAB™ computes the minimization. So we must account for this and change the MATLAB™ implementation into a maximization (see Equation 5.2). Hence, we have input $\boldsymbol{f}$ as negative values. Another observation is that we need the input function $\boldsymbol{f}$ to be a vector, so the power matrix discussed previously must be vectorized to a column vector so that $\boldsymbol{f}^{\mathrm{T}}$ is a row vector. The definition of $\boldsymbol{x}$ vector indicates which BSs are connected to which UE position with the set of active BSs. As a result, the $\boldsymbol{f}$ vector and $\boldsymbol{x}$

vector read as follows.

$$\boldsymbol{f} = \begin{bmatrix} -P(1,1) \\ -P(2,1) \\ \vdots \\ -P(B,1) \\ -P(1,2) \\ -P(2,2) \\ \vdots \\ -P(1,U) \\ \vdots \\ -P(B,U) \\ \mathbf{0}_B \end{bmatrix}, \quad \boldsymbol{x} = \begin{bmatrix} G_{\text{act}}(1,1) \\ G_{\text{act}}(2,1) \\ \vdots \\ G_{\text{act}}(B,1) \\ G_{\text{act}}(1,2) \\ G_{\text{act}}(2,2) \\ \vdots \\ G_{\text{act}}(1,U) \\ \vdots \\ G_{\text{act}}(B,U) \\ q_1 \\ q_2 \\ \vdots \\ q_B \end{bmatrix}$$

where $\mathbf{0}_B$ is the $B \times 1$ all zero vector. The $\boldsymbol{q}$ values at the end indicate which BSs will be activated according to Equation 5.3d and Equation 5.3e. The B 0's at the end of the $\boldsymbol{f}$ vector are present to nullify the $\boldsymbol{q}$ values in $\boldsymbol{x}$, as $\boldsymbol{q}$ values need not be maximized but are introduced from the constraints.

Here, we implement the equality conditions in MATLAB™. The equality matrices $\boldsymbol{A}_{\text{eq}}$ and $\boldsymbol{b}_{\text{eq}}$ are discussed first, then followed by the inequality condition. The equality conditions are given by Equation 5.3c and Equation 5.3e.The $\boldsymbol{A}_{\text{eq}}$ matrix and $\boldsymbol{b}_{\text{eq}}$ read as follows.

$$\boldsymbol{A}_{\text{eq}} = \begin{bmatrix} 1 & \cdots & 1 & 0 & \cdots & \cdots & \cdots & \cdots & \cdots & 0 \\ 0 & \cdots & 0 & 1 & \cdots & 1 & \cdots & 0 & \cdots & 0 \\ \vdots & \vdots & \vdots & \vdots & \ddots & \ddots & \ddots & \vdots & \vdots & \vdots \\ 0 & \cdots & 0 & 0 & \cdots & 0 & \cdots & 1 & \cdots & 1 \end{bmatrix}, \quad \boldsymbol{b}_{\text{eq}} = \begin{bmatrix} 1 \\ 1 \\ \vdots \\ 1 \\ k \end{bmatrix}$$

We have two inequality conditions as mentioned in Equation 5.3d and Equation 5.3f. This will be the basis for the $\boldsymbol{A}$ matrix in the function definition. Combining them into a single matrix that reads as follows.

$$\boldsymbol{A} = \begin{bmatrix} 1 & 0 & \cdots & 0 & 1 & 0 & \cdots & -U & 0 & \cdots & 0 \\ 0 & 1 & \cdots & 0 & 0 & 1 & \cdots & 0 & -U & \cdots & 0 \\ \vdots & \vdots & \vdots & \vdots & \vdots & \vdots & \vdots & \vdots & \vdots & \vdots & \vdots \\ 0 & 0 & \cdots & 1 & 0 & 0 & \cdots & 0 & 0 & \cdots & -U \\ P(1,1) & P(2,1) & \cdots & P(B,1) & 0 & 0 & \cdots & 0 & 0 & \cdots & 0 \\ 0 & 0 & \cdots & 0 & P(1,2) & P(2,2) & \cdots & 0 & 0 & \cdots & 0 \end{bmatrix}$$

Although the matrix looks overwhelming, there is a simpler way to construct this. The dimensions of this matrix is $(B + U + 1) \times (B(U + 1))$. The first B rows and the next U+1 rows can be separated into the joining of two matrices with conditions mentioned in the equations discussed earlier. This combination was done to satisfy both inequality constraints, as MATLAB™ only accepts one

parameter. The $\boldsymbol{b}$ matrix should contain values from the right side of inequalities, in which we implement the power threshold T. It reads as described below.

$$\boldsymbol{b} = \begin{bmatrix} 0 & 0 & \dots & 0 & -T & -T & \dots & -T \end{bmatrix}^{\mathrm{T}}$$

$$\mathcal{I} = \{1, 2, ..., (U+1)B\}$$

The $\mathcal{I}$ is a set indicating the indexes of integer constraints on the $\boldsymbol{x}$ vector. In this programming, we have $(U+1)B$ variables, and all of them are integers. The upper and lower bounds are also vectors and, in this case, are all 0's and 1's, respectively.

5.1.4 Result Analysis

The MILP solver, after the completion of its computation, gives the maximum mean power achievable in this system setting. It also gives us what values of the vector $\boldsymbol{x}$ we achieve this result. We call attention to the vector $\boldsymbol{x}$ with dimensions $U(B+1) \times 1$, where U and B are the same as in the previous section. The first UB cells indicate whether the direct link state is active or inactive. The last B cells show us which k BSs are chosen to achieve this result. Knowing how $\boldsymbol{x}$ is designed, we can go back and obtain the solved $\boldsymbol{G}_{\text{act}}$ matrix, which gives the information of selected communication links. A Hadamard product of $\boldsymbol{G}_{\text{act}}$ and $\boldsymbol{P}$ matrices gives us the received power from that selected direct link. We can also interpret this result in another manner. We have numerical data to support the optimum location to deploy BSs in an indoor environment. It is inherent that the optimum criteria are based on mean received power over the UE trajectory. To provide the readers with more clarity, we put forth some tables as examples of mentioned matrices, namely $\boldsymbol{G}_{\text{act}}$, $\boldsymbol{P}$, and $\boldsymbol{q}$ matrices.

$\boldsymbol{G}_{\text{act}}$	BS 1	BS 2	BS 3	BS 4	BS 5
UE position 1	1	0	0	0	0
UE position 2	0	1	0	0	0
UE position 3	1	0	0	0	0
UE position 4	0	0	1	0	0
UE position 5	0	0	0	1	0

Table 5.1: An example of $\boldsymbol{G}$ matrix

We provide an example that one activates four BSs out of five tentative deployed BSs. Using Equations 5.2 to 5.3f, a worked-out example for a test case is to be found here. To follow Equation 5.3c, the sum of the elements in each column of $\boldsymbol{G}_{\text{act}}$ matrix answers how many BSs serve one UE position, and it has to be one. The sum of the elements in each row of $\boldsymbol{G}_{\text{act}}$ answers how many UE positions are served by one BS. As stated in Equation 5.3d, it has to be less or equal to the total number of UE positions, i.e., U. From Table 5.1, one can find out that one UE position is only served by one direct link, i.e., to the BS. Every value in Table 5.2 is the received power at the UE via the direct link, and the unit is dBm.

$\boldsymbol{P}$	BS 1	BS 2	BS 3	BS 4	BS 5
UE position 1	-50	-52	-55	-58	-63
UE position 2	-48	-46	-59	-60	-64
UE position 3	-47	-53	-53	-54	-60
UE position 4	-49	-50	-43	-59	-250
UE position 5	-60	-59	-57	-40	-250

Table 5.2: An example of $\boldsymbol{P}$ matrix

BS 1	1
BS 2	1
BS 3	1
BS 4	1
BS 5	0

Table 5.3: An example of $\boldsymbol{q}$ matrix

The direct link selection is based on the $\boldsymbol{P}$ matrix, which can be proven by the comparison between Table 5.1 and Table 5.2. One can observe that BS 5 is not serving any UE, so BS 5 is not activated in Table 5.3.

After running the program for different values of k, ranging from 1 to 16, we could make comparisons or trade-offs we wish to achieve. It is important to note that for every iteration of k, the optimization goal is to maximize the mean received power for a specific minimum received power threshold (T). We start with a very small value of T and keep increasing the value of T by 1 dB. Another observation while increasing T is the decrease in the mean received power, which can be seen in the Pareto boundary figures. Here, we provide the Pareto boundaries for 3, 4, 5, and 6 active BSs. More Pareto boundaries can be found in the Appendix Figure A.4 to Figure A.15. We can see the improvement in average received power or SNR in increasing the number of BSs from Figure 5.4a to Figure 5.4d. If we increase the number of BSs, we will obviously see an improvement in mean received power at UE, but the expense of a BS must justify the performance improvement. Then, we plot the maximum mean received power and minimum received power in Figure 5.5a and Figure 5.5b, respectively. It is important to note that there is no cooperation between BSs, i.e., each UE is served by a single BS. The other case is clearly of interest but not pursued here. It can be easily accommodated into the MILP formulation.

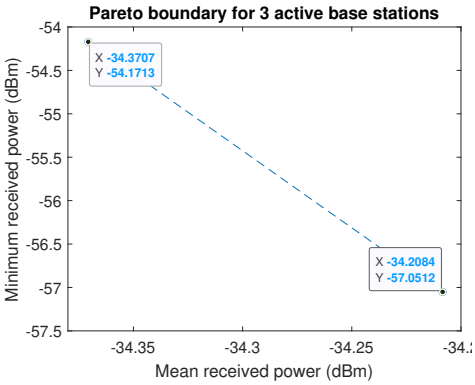

(a) Pareto boundary for 3 active BSs

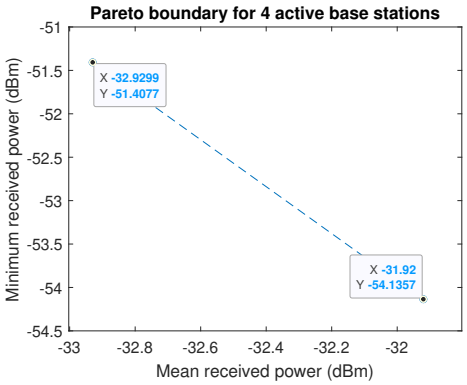

(b) Pareto boundary for 4 active BSs

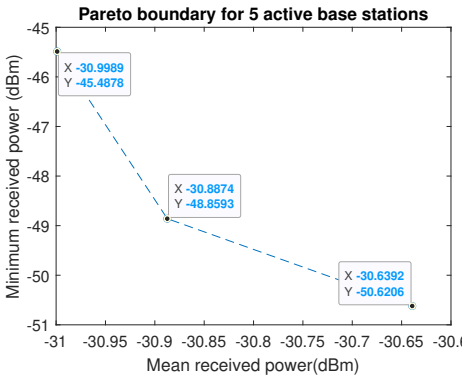

(c) Pareto boundary for 5 active BSs

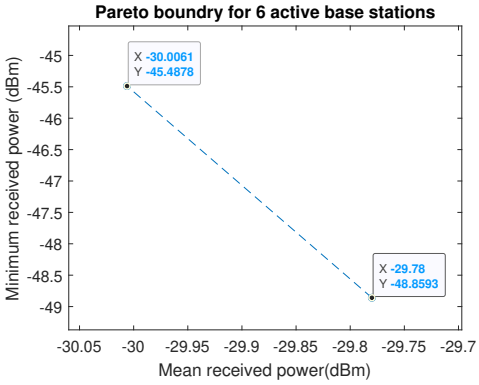

(d) Pareto boundary for 6 active BSs

Figure 5.4: Pareto boundaries

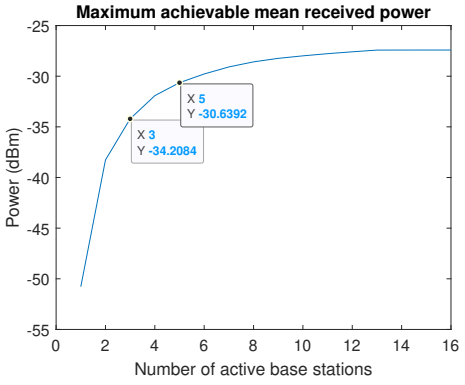

(a) Maximum mean received power mode

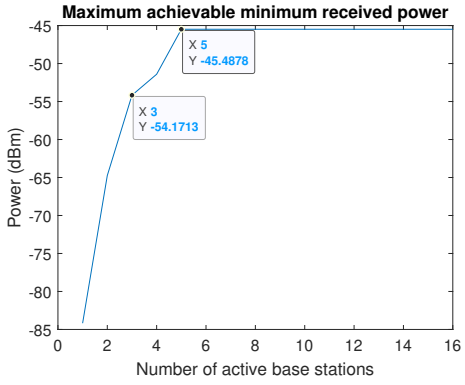

(b) Maximum minimum received power mode

Figure 5.5: Optimization results

Here, we draw some conclusions based on the upper boundaries given by the MILP solver:

- Increasing one more BS may not be worth the price, i.e., increasing the BSs from 4 to 5 only enhances the mean received power by less than 1 dB.
- Increasing the power threshold, represented by the minimum received power in the figures, leads to a degradation in mean received power.
- The MILP solver of MATLAB™ obtains the same optimum solutions as the results of the exhaustive search (see Figure 5.2 and Figure 5.4a).
- Employing standard optimization packages to find the optimum solutions significantly reduces computation complexity.
- An upper limit in mean received power arises after reaching 12 active BSs, and an upper limit in minimum received power arises after reaching 5 active BSs (see Figure 5.5a and Figure 5.5b).
- In other words, we cannot see any improvement in the threshold for having more than 5 BSs and no improvement in mean received power after 12 BSs.

5.2 Optimization for Outage Thresholds

From the power efficiency perspective, allowing an outage probability, that is, dropping some UEs with bad channel conditions, is beneficial. Therefore, a proper outage threshold is critical for the modern communication system. In this section, we solve this optimization problem for outage thresholds. Unlike the optimization of BS selection and direct link selection, the selection of dropped UE position makes the computation complexity explode. Therefore, this optimization problem can not be solved by exhaustive search because of its complexity. Hence, we only provide the results from the MILP solver.

5.2.1 Mathematical Model of Optimization

Due to the virtue of MATLAB™'s built-in function 'intlinprog,' we modeled this optimization problem in the same fashion as Equations (5.2) to (5.3e). However, the primary goal is changed to find the maximum power threshold with $P_{\text{outage}}\%$ outage probability. Two more variables are introduced to achieve this goal: outage indicator $\boldsymbol{O}$ and threshold T_{outage}. The outage indicator $\boldsymbol{O}$ comprises U elements, and each element $O(n)$ indicates whether the nth UE is dropped or not. A '1' in $O(n)$ indicates that the nth UE is dropped.

$$\max_{q_b, G_{\text{act}}(n,b), O(n)} T_{\text{outage}} \tag{5.5}$$

$$\text{subject to } G_{\text{act}}(n,b) \in \{0,1\} \tag{5.6a}$$

$$q_b \in \{0,1\} \tag{5.6b}$$

$$O(n) \in \{0,1\} \tag{5.6c}$$

$$\sum_{b=1}^{B} G_{\text{act}}(n,b) = 1 \quad \forall n \tag{5.6d}$$

$$\sum_{n=1}^{U} G_{\text{act}}(n,b) \leq q_b U \quad \forall b \tag{5.6e}$$

$$\sum_{b=1}^{B} q_b = k \tag{5.6f}$$

$$\sum_{n=1}^{U} O(n) \leq P_{\text{outage}}\%U \tag{5.6g}$$

$$\sum_{n=1}^{U} G_{\text{act}}(n,b) P(n,b) \geq T_{\text{outage}} - wO(n) \quad \text{where} \quad w \gg 1 \tag{5.6h}$$

Equation 5.5 is the new optimization target. One can see more conditions, such as Equations 5.6g to 5.6h. As mentioned, each dropped UE position is represented by a '1' in the outage indicator $\boldsymbol{O}$. Hence, the summation of all outage indicators gives the total number of dropped UE positions, shown in Equation 5.6g. The approach to allowing some UE positions in outage is to break the power threshold constraint for these UE positions in outage. Therefore, a very large value w is employed in Equation 5.6h.

5.2.2 MATLAB™ Implementation of Optimization

In this optimization problem, the optimized factors are the communication links, the combination of BSs, the UE positions in outage, and the outage threshold. Hence, we put vectorized direct link indicator $\boldsymbol{G}_{\text{act}}$, BS indicator $\boldsymbol{q}$, outage indicator $\boldsymbol{O}$, and outage threshold T_{outage} in the $\boldsymbol{x}$ matrix. As mentioned, $\boldsymbol{f}$ indicates the optimization target. We only target to maximize the outage threshold, achieved by giving zeros except for the last value in the $\boldsymbol{f}$ matrix. As we have one more indicator in this optimization problem, we provide how to define the outage indicator $O(n)$. Since the optimization target is also changed, we must change $\boldsymbol{x}$ and $\boldsymbol{f}$. Along with the definition of $\boldsymbol{O}$, $\boldsymbol{x}$ and $\boldsymbol{f}$, they read as follows:

$$\boldsymbol{O} = \begin{bmatrix} O(1) & O(2) & \cdots & O(U-1) & O(U) \end{bmatrix}$$

$$\boldsymbol{f} = \begin{bmatrix} \mathbf{0}_{B+U+BU} \\ 1 \end{bmatrix}, \quad \boldsymbol{x} = \begin{bmatrix} G_{\text{act}}(1,1) \\ \vdots \\ G_{\text{act}}(B,1) \\ G_{\text{act}}(1,2) \\ \vdots \\ G_{\text{act}}(1,U) \\ \vdots \\ G_{\text{act}}(B,U) \\ q_1 \\ \vdots \\ q_B \\ O(1) \\ \vdots \\ O(U) \\ T_{\text{outage}} \end{bmatrix}$$

5.2.3 Result analysis

In accordance with the structure of $\boldsymbol{x}$, one can extract the first BN values and reshape them as a $B \times U$ matrix, which is the output $\boldsymbol{G}_{\text{act}}$ matrix. Then, the following B values can form the $\boldsymbol{q}$ matrix. Moreover, one can take the next U values as outage indicators, that is, $\boldsymbol{O}$. As a result, the last value in $\boldsymbol{x}$ is the optimized outage threshold T_{outage}.

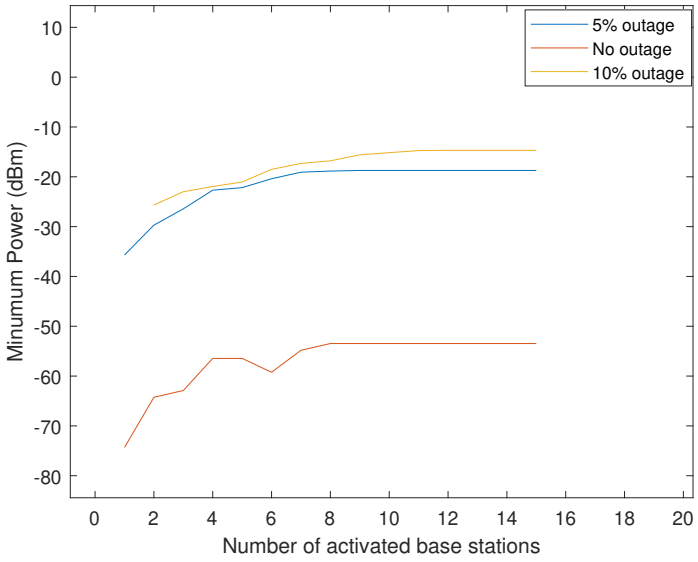

Figure 5.6: System performance under different outage probability

With different numbers of BSs, we optimized the outage thresholds for outage probabilities of 0%, 5%, and 10%, respectively. Notably, this optimization problem is very complex and consumes a massive amount of resources. Therefore, we set an upper limit on the run time. One can observe some imperfections in the results given by the MILP solver.

In Figure 5.6, the red curve shows the optimized power thresholds with 0% outage probability, the blue curve shows the optimized power thresholds with 5% outage probability, and the gold curve shows the optimized power thresholds with 10% outage probability. The values in the x-axis refer to the number of activated BSs, and the values in the y-axis refer to the power with the unit of dBm. With only one activated BS, one can observe one imperfection in Figure 5.6: dropping 10% of UE positions even degrades the system performance (see the gold curve). It is because the MILP solver requires more resources to search for a reasonable result. Increasing the outage probability from 0% to 5%, one can observe a great improvement in power thresholds. However, one can not observe any significant difference between 10% outage probability and 5% outage probability. Moreover, the outage threshold also converges to an upper limit after reaching nine activated BSs.

As 5% outage probability greatly improves the power thresholds, we focus on 5% outage probability and provide more optimization results such as mean received power, minimum received power, and QoS.

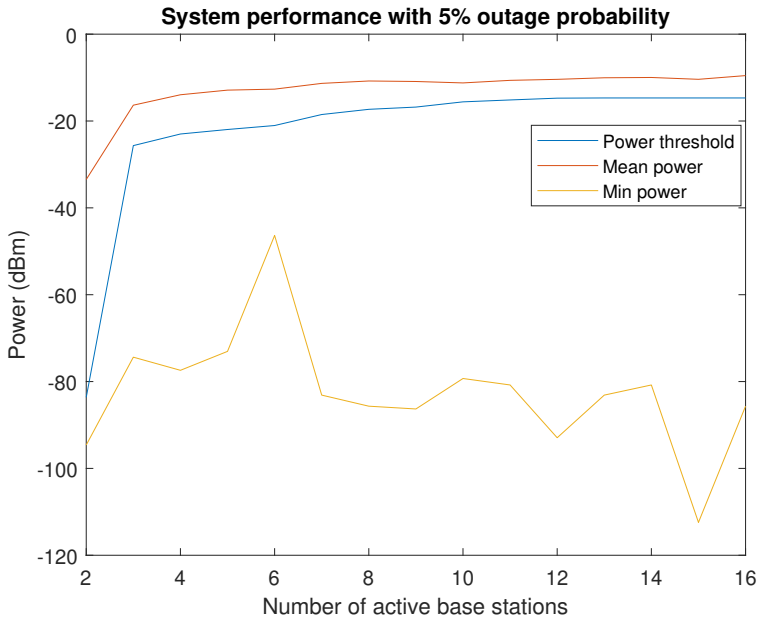

Figure 5.7: System performance with 5% outage probability

In Figure 5.7, the red curve shows the mean received power at the UE position, the blue curve shows the optimized power threshold, and the gold curve shows the

minimum received power. One can see that the gold curve varies significantly, which proves some UE positions are in outage. We can explain more specifically. Once one UE position is in outage, the power threshold constraint is no longer valid for this UE position. Hence, the received power at the dropped UE position is much lower than the optimized power threshold and varies significantly. Moreover, the mean received power and power threshold grow with the increased number of activated BSs.

As mentioned, allowing an outage probability is beneficial with respect to power efficiency. In another aspect, the QoS is also essential for both UEs and network operators. Driven by this concern, we also investigated the QoS with a 5% outage probability. We provide the QoS with two, three, four, five, eight, and nine activated BSs from Figure 5.8a to Figure 5.8f. More figures are in the Appendix (Figure A.16). Deploying two BSs, one can easily observe that the QoS is extremely unstable (see Figure 5.8a). But, Figure 5.8b shows that only one more BS can stabilize the QoS. While increasing the active BSs, one can see that the QoS is more and more stable.

Here, we give some conclusions based on the results mentioned above:

- Dropping some UE positions with bad communication conditions can enhance the system performance regarding mean received power and power threshold.
- 5% outage probability is generally the best choice considering the trade-off between power efficiency and QoS.
- Three BSs is a minimum requirement to provide stable QoS in this ray tracing simulation.
- Outage power threshold converges to an upper limit after reaching nine active BSs.

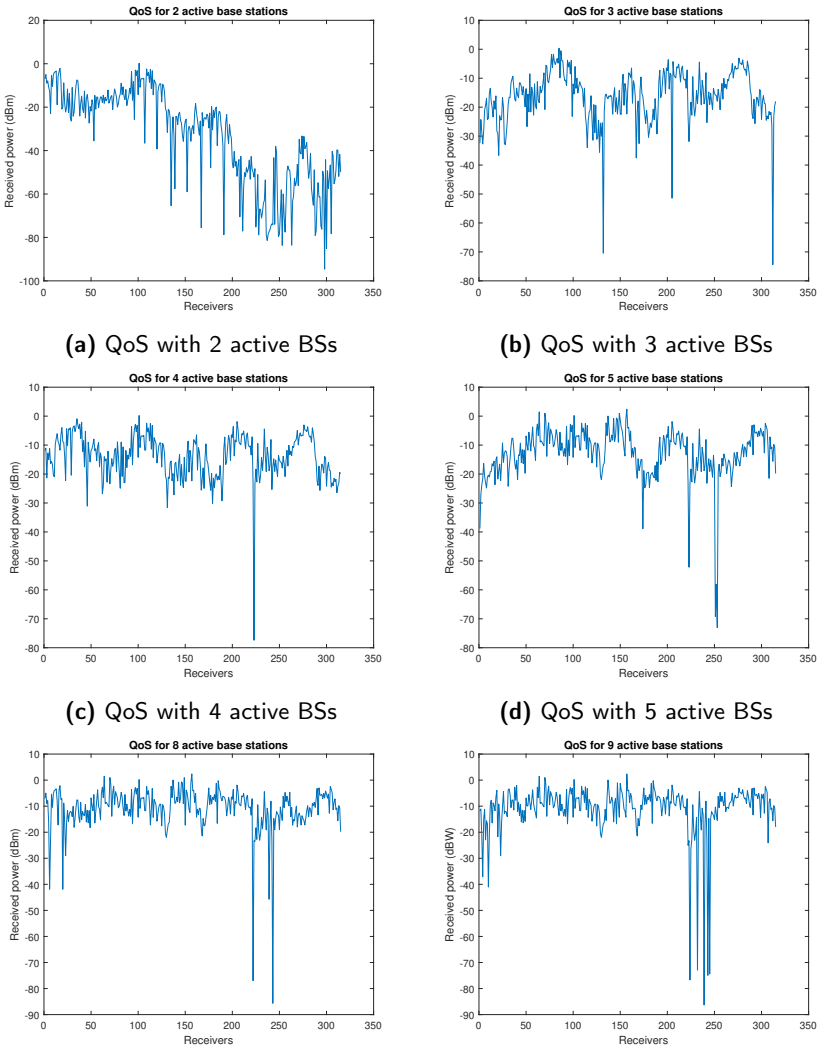

(a) QoS with 2 active BSs

(b) QoS with 3 active BSs

(c) QoS with 4 active BSs

(d) QoS with 5 active BSs

(e) QoS with 8 active BSs

(f) QoS with 9 active BSs

Figure 5.8: QoS with 5% outage probability

5.3 Optimization for RIS-assisted Communication System

The optimum link selection in RIS-assisted communication is similar to the direct link case. The similarity lies in our approach to the solution. We use MILP to determine which BSs and RIS positions must be selected for the best performance. However, the difference comes in the mathematical framework of the problem and will be discussed in the following section.

5.3.1 Mathematical Model

As mentioned before, the difference between a direct link selection and RIS-assisted link selection is in the mathematical framework of the optimization problem. The goal remains to maximize the mean received power for all the UE positions in the trajectory from Figure 4.1. But now we have the RIS also as a variable. This additional variable is responsible for a three-dimensional activation matrix $G_{\text{act}}(b, r, n)$ compared to a two-dimensional one in Section 5.1. Hence the optimization problem can be formulated as in Equation 5.7.

$$\max_{q_b, q_r, G_{\text{act}}(b,r,n)} \sum_{b=1}^{B} \sum_{r=1}^{R} \sum_{n=1}^{U} G_{\text{act}}(b, r, n) P(b, r, n) \tag{5.7}$$

$$\text{subject to } G_{\text{act}}(b, r, n) \in \{0, 1\} \tag{5.8a}$$

$$q_b \in \{0, 1\} \tag{5.8b}$$

$$q_r \in \{0, 1\} \tag{5.8c}$$

$$\sum_{b=1}^{B} q_b = k \tag{5.8d}$$

$$\sum_{r=1}^{R} q_r = i \tag{5.8e}$$

$$\sum_{b=1}^{B} \sum_{r=1}^{R} G_{\text{act}}(b, r, n) = 1 \quad \forall n \tag{5.8f}$$

$$\sum_{r=1}^{R} \sum_{n=1}^{U} G_{\text{act}}(b, r, n) \leq URq_b \quad \forall l \tag{5.8g}$$

$$\sum_{b=1}^{B} \sum_{n=1}^{U} G_{\text{act}}(b, r, n) \leq UBq_r \quad \forall r \tag{5.8h}$$

$$\sum_{b=1}^{B} \sum_{r=1}^{R} G_{\text{act}}(b, r, n) P(b, r, n) \geq T \quad \forall n \tag{5.8i}$$

The methodology to obtain the channel gain in the presence of a RIS has been explained in Section 4.5 and used here to obtain the received power at every UE location from all possible communication links, including both direct links and

RIS-assisted links. The optimization problem has been elaborated along with constraints in Equations 5.7 and 5.8a - 5.8i. In Equation 5.7, B,R,U indicate the number of BSs, RIS, and UE positions considered when evaluating the maximization. $\boldsymbol{G}_{\text{act}}$ is the activation matrix and $\boldsymbol{P}$ is received power in matrix format. Similar to the optimization in direct link selection, we have constraints shown in Equations 5.8a - 5.8i.

In Equations 5.8a to 5.8c, 0 indicates an "off" state or the link is inactive, and 1 indicates an "on" state or the link is active. i and k denote the number of active RISs and BSs, respectively. We have a format to compare the obtained results across different values for these variables. As mentioned in earlier sections, we have constrained the UE to be served by a single link which can be seen in Equation 5.8f. The constraints in Equations 5.8g and 5.8h indicate the maximum number of possible links using a single BS and a single RIS respectively. The equality present in Equation 5.8g refers to the extreme case where only a single BS b might be chosen to serve all the UE positions using different RISs in the environment. The inequality indicates the relaxed versions of the extreme case. It can also be understood mathematically that for a specific value of b, the summation in Equation 5.8g can take a maximum value of UR as q_b can either be 0 or 1. Equation 5.8h also follows a similar definition as Equation 5.8g.

5.3.2 MATLAB™ Implementation

MILP problems are solved using the "intlinprog" in-built function. The similarity between the RIS-assisted link selection and the direct link selection allows us to implement the problem in the same format, but the matrices have different dimensions. This section will show how the elements have been reordered to be applied in Equation 5.4. The three-dimensional power matrix has been split into individual two-dimensional matrices and can be observed in the matrix below.

$$\boldsymbol{P(:,:,1)} = \begin{bmatrix} P(1,1,1) & P(1,2,1) & \cdots & P(1,U-1,1) & P(1,U,1) \\ P(2,1,1) & P(2,2,1) & \cdots & P(2,U-1,1) & P(2,U,1) \\ \vdots & \vdots & \ddots & \vdots & \vdots \\ P(B-1,1,1) & P(B-1,2,1) & \cdots & P(B-1,U-1,1) & P(B-1,U,1) \\ P(B,1,1) & P(B,2,1) & \cdots & P(B,U-1,1) & P(B,U,1) \end{bmatrix}$$

$$\boldsymbol{P(:,:,2)} = \begin{bmatrix} P(1,1,2) & P(1,2,2) & \cdots & P(1,R-1,2) & P(1,R,2) \\ P(2,1,2) & P(2,2,2) & \cdots & P(2,R-1,2) & P(2,R,2) \\ \vdots & \vdots & \ddots & \vdots & \vdots \\ P(B-1,1,2) & P(B-1,2,2) & \cdots & P(B-1,R-1,2) & P(B-1,R,2) \\ P(B,1,2) & P(B,2,2) & \cdots & P(B,R-1,2) & P(B,R,2) \end{bmatrix}$$

$$\vdots$$

$$\boldsymbol{P(:,:,U)} = \begin{bmatrix} P(1,1,U) & P(1,2,U) & \cdots & P(1,R-1,U) & P(1,R,U) \\ P(2,1,U) & P(2,2,U) & \cdots & P(2,R-1,U) & P(2,R,U) \\ \vdots & \vdots & \ddots & \vdots & \vdots \\ P(B-1,1,U) & P(B-1,2,U) & \cdots & P(B-1,R-1,U) & P(B-1,R,U) \\ P(B,1,U) & P(B,2,U) & \cdots & P(B,R-1,U) & P(B,R,U) \end{bmatrix}$$

$P(b,r,n)$ for $\forall\ n$ is a single element from the power matrix containing the received power from the bth BS utilizing rth RIS to the nth UE position. When we provide this to intlinprog, it must be vectorized to a column vector. This vectorized form of the received power can be seen in the $\boldsymbol{f}$ vector below. We recall that zeros have been appended at the end of the $\boldsymbol{f}$ vector to account for other variables in the solution. In the RIS-assisted link, we need $B + R$ zeros at the end to account for q_B and q_R matrices. The zero-padded vectors are $\mathbf{0}_B$ and $\mathbf{0}_R$ and can be seen at the end of the $\boldsymbol{f}$ vector:

$$\boldsymbol{f} = \begin{bmatrix} -P(1,1,1) \\ \vdots \\ -P(B,1,1) \\ -P(1,2,1) \\ \vdots \\ -P(B,2,1) \\ \vdots \\ -P(B,R,1) \\ \vdots \\ -P(B,R,2) \\ \vdots \\ -P(B,R,U) \\ \mathbf{0}_B \\ \mathbf{0}_R \end{bmatrix}$$

The activation matrix is also three-dimensional and is vectorized to input in Equation 5.4 as $\boldsymbol{x}$. Using intlinprog, we arrive at values for $\boldsymbol{x}$, which maximize the average received power across all UE positions. This vector $\boldsymbol{x}$ has the following structure and is further explained below.

$$\boldsymbol{x} = \begin{bmatrix} -G_{\text{act}}(1,1,1) \\ \vdots \\ -G_{\text{act}}(B,1,1) \\ -G_{\text{act}}(1,2,1) \\ \vdots \\ -G_{\text{act}}(B,2,1) \\ \vdots \\ -G_{\text{act}}(B,R,1) \\ \vdots \\ -G_{\text{act}}(B,R,2) \\ \vdots \\ -G_{\text{act}}(B,R,U) \\ q_B(1) \\ \vdots \\ q_B(B) \\ q_R(1) \\ \vdots \\ q_R(R) \end{bmatrix}$$

The vector $\boldsymbol{x}$ has the following structure.

- Vectorized activation matrix $\boldsymbol{G}_{\text{act}}$.
- Selection vector for BSs. This vector indicates which k BSs are active from the B available ones in the simulation environment.
- Selection vector for RIS. This vector indicates which i RISs are active from the R available ones in the simulation environment.

The equality and inequality conditions have also been incorporated as rows in a matrix to provide inputs for $\boldsymbol{A}$,$\boldsymbol{A}_{\text{eq}}$,$\boldsymbol{b}$,$\boldsymbol{b}_{\text{eq}}$ in Equation 5.4. These matrices have huge sizes, so we do not wish to detail them here.

5.3.3 Result Analysis

As mentioned in the previous section, intlinprog answers the variables in vector $\boldsymbol{x}$. The first BRN entries belong to the activation matrix indicating which BS using which RIS serves a particular UE. As we have vectorized the activation matrix in MATLAB™, we can use the reverse of that method to obtain the answer to the activation matrix in a 3-dimensional format. The last R entries indicate the selection vector for RISs, and the remaining entries belong to the selection vector for BSs. This can also be seen in the $\boldsymbol{x}$ vector in the previous section.

Here, we provide surface plots calculated by the ray tracing simulation with 0 dBm input power. Each RIS has 144 elements. It is noteworthy that one can observe the results with different power amplifications in the following figures. Looking back to our RIS structure in Figure 3.3, one power amplifier is employed. We provide the results with two different power amplifications, which are 24 dB and 26 dB. In the following surface plots, the values on the y-axis represent the number of activated BSs; the x-axis represents the number of activated RISs, and the z-axis represents the power with the unit of dBm.

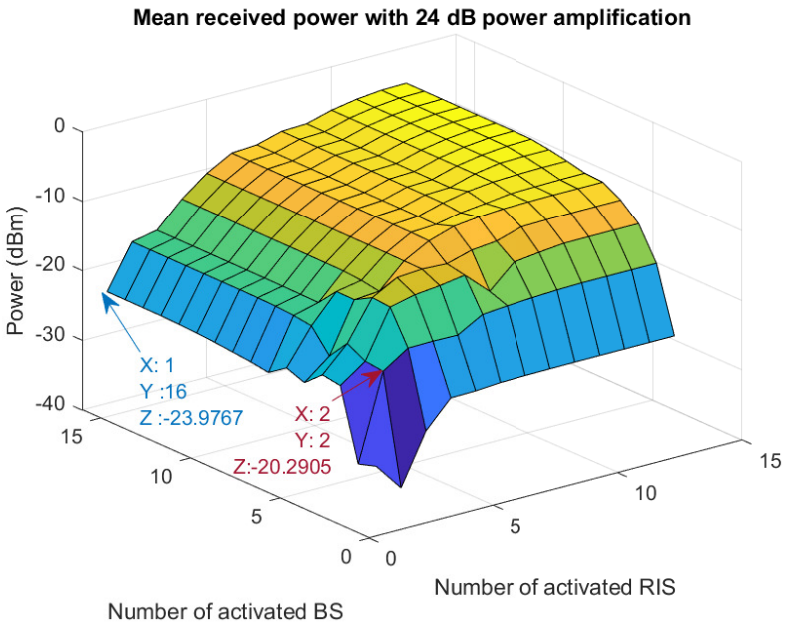

Figure 5.9: Mean received power with 24 dB power amplification

After applying 24 dB power amplification in every RIS, we can get the mean received power under the maximum achievable power threshold constraint (see Figure 5.9). The cut of this with 0 RIS can be seen in Figure 5.4a to Figure 5.4d and the Appendix (Figure A.4 to A.15), where no RIS deployed. Thus, a comparison to the previous chapter is already in the figures. The target trade-offs can be viewed jointly in Figure 5.9 and 5.10. As shown, one can achieve a mean received power of -20.29 dBm with two BSs and two RISs. In the meantime,

deploying sixteen BSs and 1 RIS only achieves a mean received power of -23.98 dBm. Instead of deploying sixteen BSs, one can remove fourteen BSs and deploy one more RIS in a proper position. As a result, one can improve the system performance at a lower cost. One can also observe a plateau, a saturation region in Figure 5.9. It means the upper limit of mean received power can be achieved without exhausting all the BS and RIS resources. In this simulation, deploying eight BSs and eleven RISs is sufficient to reach the upper limit on mean received power, which enables one to find a good compromise between the number of RISs and the number of BSs.

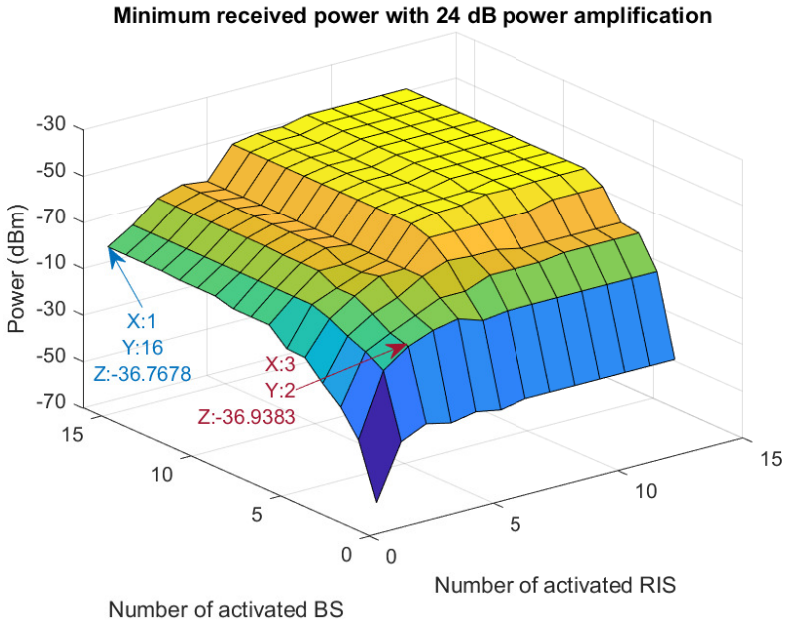

Figure 5.10: Minimum received power with 24 dB power amplification

Figure 5.10 shows the surface plot of the minimum received power, in which some trade-offs can also be found. As shown, deploying sixteen BSs and one RIS can achieve a minimum power of -36.77 dBm, which can also be achieved by deploying two BSs and three RISs. Same as Figure 5.9, one can also observe a plateau in Figure 5.10. It indicates that the upper limit of minimum received power can be achieved by eight BSs and nine RISs.

The surface plots with 26 dB power amplification can be found in Figure 5.11 and Figure 5.12. Some blank space arises due to the lack of computation resources. One can observe that the upper limits of mean and minimum received power are all improved, which tells the upper limit of performance can be improved by increasing the power amplification of RISs.

Here, we draw some conclusions based on the results and analysis given in this optimization problem:

- Deploying RISs can reduce the number of BSs without any loss regarding the mean and minimum received power performance.
- Deploying RISs can not bring any improvement if too few BSs are present.
- The trade-offs between the number of BSs and the number of RISs can be found in surface plots (Figure 5.9 to Figure 5.12).
- The upper limit of system performance can be achieved before exhausting all BSs and RISs in this simulation.
- The upper limit of system performance can be improved by increasing the power amplification of RISs.

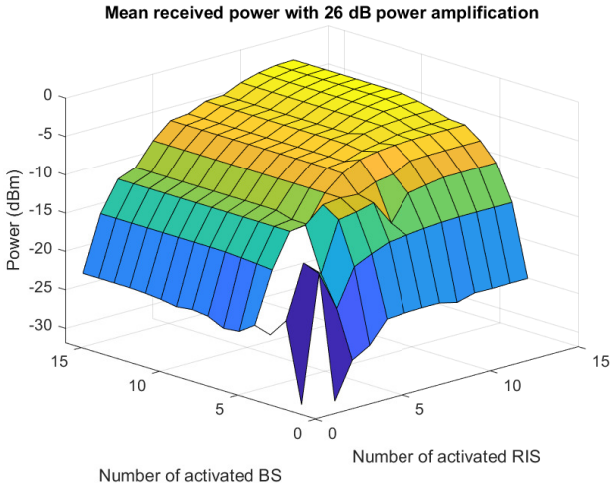

Figure 5.11: Mean received power with 26 dB power amplification

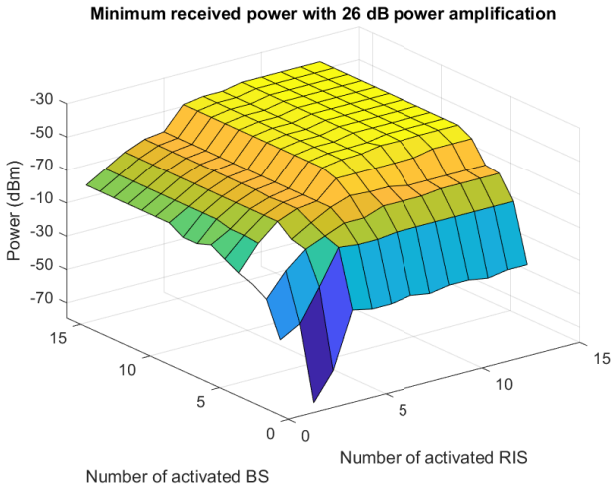

Figure 5.12: Minimum received power with 26 dB power amplification

5.4 Optimising Phase

Previously, we have provided information about trade-offs in received power versus the number of BSs in direct link optimization and discussed achieving these results using the exhaustive search. We have also mentioned why exhaustive search becomes increasingly complex in RIS-assisted links. The previous section covered the power trade-off with increasing BSs and RISs. It is important to note that the phase shift within the RIS is applied on both sides, i.e., towards the transmitter and receiver, and can be seen in Figure 3.3. In the following subsection, we explain how phase was calculated until this point and provide some information on how to do it in the case of a wideband system.

5.4.1 Phase calculation in RIS - Narrowband

Using the Narrowband assumption, we have obtained the channel transfer function in RIS-assisted link as explained in Section 4.5.1. In Equation 4.7, we observe the presence of θ_i and ϕ_j, denoted as the phase compensation applied in the RIS. i and j in θ_i and ϕ_j denote the RIS element. As mentioned in Section 4.5.1, the channel between BS and RIS was modeled as a SIMO system, and the channel between RIS and UE position as a MISO system. The channel coefficients take the form of Equations 4.5 and 4.6 for the SIMO and MISO cases. The complex weighted vectors containing the values of θ_i and ϕ_j, can be denoted as vectors $\boldsymbol{V}_1$ and $\boldsymbol{V}_2$ in Equations 5.9 and 5.10

$$\boldsymbol{V}_1 = \begin{bmatrix} \exp(j\theta_1) & \exp(j\theta_2) & \cdots & \exp(j\theta_m) \end{bmatrix} \tag{5.9}$$

$$\boldsymbol{V}_2 = \begin{bmatrix} \exp(j\phi_1) & \exp(j\phi_2) & \cdots & \exp(j\phi_m) \end{bmatrix}^{\mathrm{T}} \tag{5.10}$$

Vectors $\boldsymbol{V}_1$ and $\boldsymbol{V}_2$ have dimensions $1{\times}m$ and $m{\times}1$. To maximize the individual vector products in Equation 4.7, we would like to have

$$\theta_i = -\arg(h_{\text{txi}}),\ \ i = \{1, 2, \cdots, N\} \tag{5.11a}$$

$$\phi_j = -\arg(h_{\text{rxi}}),\ \ j = \{1, 2, \cdots, N\} \tag{5.11b}$$

where arg is the argument of the complex number and m is the total number of elements in the RIS. With phase values as in Equations 5.11a and 5.11b, the product $h_{\text{txi}}\exp(j\theta_i)$ and $h_{\text{rxi}}\exp(j\phi_i)$ becomes

$$h_{\text{txi}}\exp(j\theta_i) = \text{abs}(h_{\text{txi}}), \quad \text{when } \theta_i = -\arg(h_{\text{txi}}) \tag{5.12a}$$

$$h_{\text{rxi}}\exp(j\phi_j) = \text{abs}(h_{\text{rxi}}), \quad \text{when } \phi_j = -\arg(h_{\text{rxi}}) \tag{5.12b}$$

Using Equations 5.12a and 5.12b, we have reduced Equation 4.7 to Equation 5.13.

$$H_{\text{BS-RIS-UE}} = \frac{\sum_{i=1}^{m} \text{abs}(h_{\text{txi}}) \sum_{j=1}^{m} \text{abs}(h_{\text{rxi}})}{m} \tag{5.13}$$

The complex weighted vector was obtained from the phase compensation using Equations 5.11a and 5.11b can be seen in Equations 5.14 and 5.15.

$$\boldsymbol{V}_1 = \begin{bmatrix} \exp(-j\arg(h_{\text{tx1}})) & \exp(-j\arg(h_{\text{tx2}})) & \cdots & \exp(-j\arg(h_{\text{tx}m})) \end{bmatrix} \tag{5.14}$$

$$\boldsymbol{V}_2 = \begin{bmatrix} \exp(-j\arg(h_{\text{rx1}})) \\ \exp(-j\arg(h_{\text{rx2}})) \\ \vdots \\ \exp(-j\arg(h_{\text{rx}m})) \end{bmatrix} \tag{5.15}$$

The summations in Equation 4.7 can also be written as vector products using the complex weighted vectors mentioned in Equations 5.9 and 5.10. If $\boldsymbol{H}_{\text{Tx}}$ and $\boldsymbol{H}_{\text{Rx}}$ are as described in Equations 4.5 and 4.6 respectively, then the cascaded channel transfer function can be visualized as the vector product of $\boldsymbol{V}_1$, $\boldsymbol{H}_{\text{Tx}}$, $\boldsymbol{H}_{\text{Rx}}$, $\boldsymbol{V}_2$ and Equation 4.7 can be rewritten as

$$H_{\text{BS-RIS-UE}} = \frac{\boldsymbol{V}_1 \boldsymbol{H}_{\text{Tx}}}{m} \boldsymbol{H}_{\text{Rx}} \boldsymbol{V}_2 \tag{5.16}$$

It is notable to mention $H_{\text{BS-RIS-UE}}$ is a scalar value. This is how we define the cascaded channel transfer function evaluated at a single frequency point. We have not included the gain from the power amplifier present in the RIS as shown in Figure 3.3 in the above formulations. This is done to simplify our evaluations when obtaining a phase in wideband systems and can be understood in the next section.

5.4.2 Phase calculation in RIS - Wideband

In the previous section, we explained our approach for phase compensation in the narrowband scenario. The channel transfer function was evaluated for a single frequency point, i.e., the center frequency f_c at 5 GHz. When we talk about a wideband system, we mean the range of frequencies sampled 201 times with a 1 MHz spacing. In other words, the total operational bandwidth is between [4.9 GHz, 5.1 GHz] with 201 frequency samples and a 1 MHz spacing between samples.

The channel matrix for the SIMO case and the MISO case was given in Equations 4.8 and 4.9. It is important to note that the channel differs for every frequency sample and can be seen in Figure 4.4. We have also mentioned that the channel was frequency selective from observing the same figure. The point we are trying to make here is in the narrowband scenario, and we chose the phase as described in Equations 5.11a and 5.11b as we only had one channel coefficient for each antenna element. Now we have an array of channel coefficients, and we cannot say with certainty that picking one channel coefficient from this array and using it in Equations 5.11a and 5.11b is optimum. Our solution for this problem is to model it as an unconstrained optimization problem and use the "fminunc" function of MATLAB™ to arrive at two sets of phase values (for the receiving and transmitting modes) maximizing the average power over all frequency samples.

5.4.3 Mathematical model for Optimum phase and Coordinate ascent

To formulate the phase problem as an unconstrained optimization, we first need to calculate the entire channel gain for the RIS-assisted link. The channel transfer function can be written as in Equation 5.17

$$H_f = \frac{\boldsymbol{V}_1 \boldsymbol{H}_{\mathrm{Txf}}}{m} \boldsymbol{H}_{\mathrm{Rxf}} \boldsymbol{V}_2 \tag{5.17}$$

where $\boldsymbol{V}_1$ and $\boldsymbol{V}_2$ take the same form as in Equations 5.9 and 5.10 but $\boldsymbol{H}_{\mathrm{Txf}}$ and $\boldsymbol{H}_{\mathrm{Rxf}}$ are $\boldsymbol{H}_{\mathrm{Tx}}$ and $\boldsymbol{H}_{\mathrm{Rx}}$ evaluated at frequency sample f (the f^{th} column in Equation 4.8 and f^{th} row in Equation 4.9) respectively. For the sake of clarity, we would like to mention $\boldsymbol{H}_{\mathrm{Txf}}$ and $\boldsymbol{H}_{\mathrm{Rxf}}$ and matrices with dimensions $201 \times m$ and $m \times 201$.

The received power when we have the channel matrix H_f was calculated using Equation 5.18.

$$P_f = H_f H_f^{\mathrm{H}} \tag{5.18}$$

Substituting Equations 5.17 in 5.18, we arrive at Equation 5.19a.

$$P_f = \left(\frac{\boldsymbol{V}_1 \boldsymbol{H}_{\mathrm{Txf}} \boldsymbol{H}_{\mathrm{Rxf}} \boldsymbol{V}_2}{m} \right) \left(\frac{\boldsymbol{V}_1 \boldsymbol{H}_{\mathrm{Txf}} \boldsymbol{H}_{\mathrm{Rxf}} \boldsymbol{V}_2}{m} \right)^{\mathrm{H}} \tag{5.19a}$$

$$= \frac{\left(\boldsymbol{V}_1 \boldsymbol{H}_{\mathrm{Txf}} \boldsymbol{H}_{\mathrm{Rxf}} \boldsymbol{V}_2\right) \left(\boldsymbol{V}_1 \boldsymbol{H}_{\mathrm{Txf}} \boldsymbol{H}_{\mathrm{Rxf}} \boldsymbol{V}_2\right)^{\mathrm{H}}}{m^2} \tag{5.19b}$$

$$= \frac{\left(\boldsymbol{V}_1 \boldsymbol{H}_{\mathrm{Txf}} \boldsymbol{H}_{\mathrm{Rxf}} \boldsymbol{V}_2)(\boldsymbol{V}_2^{\mathrm{H}} \boldsymbol{H}_{\mathrm{Rxf}}^{\mathrm{H}} \boldsymbol{H}_{\mathrm{Txf}}^{\mathrm{H}} \boldsymbol{V}_1^{\mathrm{H}}\right)}{m^2} \tag{5.19c}$$

We can rearrange Equation 5.19c using the properties of the trace of a matrix. We are interested in two rearrangements, and they are shown in Equations 5.20a and 5.20b.

$$P_f = \mathrm{tr}\left\{\frac{\boldsymbol{V}_1(\boldsymbol{H}_{\mathrm{Txf}}\boldsymbol{H}_{\mathrm{Rxf}}\boldsymbol{V}_2)(\boldsymbol{H}_{\mathrm{Txf}}\boldsymbol{H}_{\mathrm{Rxf}}\boldsymbol{V}_2)^{\mathrm{H}}\boldsymbol{V}_1{}^{\mathrm{H}}}{m^2}\right\} \tag{5.20a}$$

$$= \mathrm{tr}\left\{\frac{\boldsymbol{V}_2^{\mathrm{H}}(\boldsymbol{V}_1\boldsymbol{H}_{\mathrm{Txf}}\boldsymbol{H}_{\mathrm{Rxf}})^{\mathrm{H}}(\boldsymbol{V}_1\boldsymbol{H}_{\mathrm{Txf}}\boldsymbol{H}_{\mathrm{Rxf}})\boldsymbol{V}_2}{m^2}\right\} \tag{5.20b}$$

The interesting aspect of these two rearrangements is that we have managed to isolate the complex weighted vectors $\boldsymbol{V}_1$ and $\boldsymbol{V}_2$ in Equations 5.20a and 5.20b. If we have a vector available for $\boldsymbol{V}_2$, we can use Equation 5.20a to find a solution for $\boldsymbol{V}_1$ and vice-versa.

From Equations 5.20a and 5.20b, we have concluded that the phase compensation provided on both the BS and UE sides directly influences the received power. Hence an optimized solution for $\boldsymbol{V}_1$ and $\boldsymbol{V}_2$ maximizing the average power over all frequency samples is possible. But as explained earlier, we need to have $\boldsymbol{V}_1$ or $\boldsymbol{V}_2$ vector available to us to solve for the other. This motivated us to use coordinate ascent to arrive at an optimum solution.

As mentioned in the previous paragraphs, we need to have knowledge of either $\boldsymbol{V}_1$ or $\boldsymbol{V}_2$ vectors. To arrive at this knowledge, we have used optimization on the BS-RIS and RIS-UE links separately to maximize average power over all frequencies. The optimization for the BS-RIS link can be seen in Equations 5.21a and 5.21b.

$$\max_{\boldsymbol{V}_1} \sum_{f=1}^{P} \mathrm{tr}\{(\boldsymbol{V}_1\boldsymbol{H}_{\mathrm{Tx}f})(\boldsymbol{V}_1\boldsymbol{H}_{\mathrm{Tx}f})^{\mathrm{H}}\} \tag{5.21a}$$

$$\text{subject to } |v_{1k}| = 1 \quad \forall k \tag{5.21b}$$

where v_{1k} is the k^{th} element in vector $\boldsymbol{V}_1$. The optimization for the RIS-UE link can be seen in Equations 5.22a and 5.22b

$$\max_{\boldsymbol{V}_2} \sum_{f=1}^{P} \mathrm{tr}\{(\boldsymbol{H}_{\mathrm{Rx}f}\boldsymbol{V}_2)(\boldsymbol{H}_{\mathrm{Rx}f}\boldsymbol{V}_2)^{\mathrm{H}}\} \tag{5.22a}$$

$$\text{subject to } |v_{2k}| = 1 \quad \forall k \tag{5.22b}$$

where v_{2k} is the k^{th} element in vector $\boldsymbol{V}_2$. The constraint present in Equations 5.21b and 5.22b is only applicable to vectors $\boldsymbol{V}_1$ and $\boldsymbol{V}_2$, but not the $\boldsymbol{\theta}$ and $\boldsymbol{\phi}$. So it is still an unconstrained optimization when we provide $\boldsymbol{\theta}$ and $\boldsymbol{\phi}$ to "fminunc" in MATLAB™. The above optimizations have been carried out to have an initial vector for $\boldsymbol{V}_1$ and $\boldsymbol{V}_2$. This initial vector must not be confused with starting position used in later paragraphs. Using these values, we can carry out the following optimization problem given in Equations 5.23a and 5.23b.

$$\max_{\boldsymbol{V}_2} \sum_{f=1}^{P} \mathrm{tr}\{\boldsymbol{V}_2^{\mathrm{H}}(\boldsymbol{V}_1\boldsymbol{H}_{\mathrm{Tx}f}\boldsymbol{H}_{\mathrm{Rx}f})^{\mathrm{H}}(\boldsymbol{V}_1\boldsymbol{H}_{\mathrm{Tx}f}\boldsymbol{H}_{\mathrm{Rx}f})\boldsymbol{V}_2\} \tag{5.23a}$$

$$\text{subject to } |v_{2k}| = 1 \tag{5.23b}$$

We use the $\boldsymbol{V}_1$ vector obtained using Equation 5.21a to compute the unknown $\boldsymbol{V}_2$ vector in Equation 5.23a. Now that we have obtained a vector $\boldsymbol{V}_2$, we use this in Equation 5.24a to obtain an optimized $\boldsymbol{V}_1$ vector.

$$\max_{\boldsymbol{V}_1} \sum_{f=1}^{P} \mathrm{tr}\{\ \boldsymbol{V}_1(\boldsymbol{H}_{\mathrm{Txf}}\boldsymbol{H}_{\mathrm{Rxf}}\boldsymbol{V}_2)(\boldsymbol{H}_{\mathrm{Txf}}\boldsymbol{H}_{\mathrm{Rxf}}\boldsymbol{V}_2)^{\mathrm{H}}\boldsymbol{V_1}^{\mathrm{H}}\} \tag{5.24a}$$

$$\text{subject to } |v_{1k}| = 1 \tag{5.24b}$$

We repeat the above-mentioned optimizations until we see no improvement in the average received power. This indicates that we have reached the local optimum and no better solution is available. It is important to note that we use the term local optimum, not global optimum. This is due to the dependence of unconstrained optimization on the starting position provided to it. This starting position must not be confused with the initial vector mentioned earlier.

5.4.4 Result Analysis

Using coordinate ascent, as mentioned in the previous section, we obtained the maximum average received power using optimized phase values. The coordinate ascent can only be applied to a single link in a RIS-assisted communication system. This statement means that the phase values for every element of the RIS are only valid for a particular BS position and UE position. If the channel changes in any manner, the calculated phase values are not optimum anymore and have to be re-evaluated. The channel gain was calculated using the phase information obtained at the center frequency, and the phase information obtained from the optimization has been plotted in Figure 5.13.

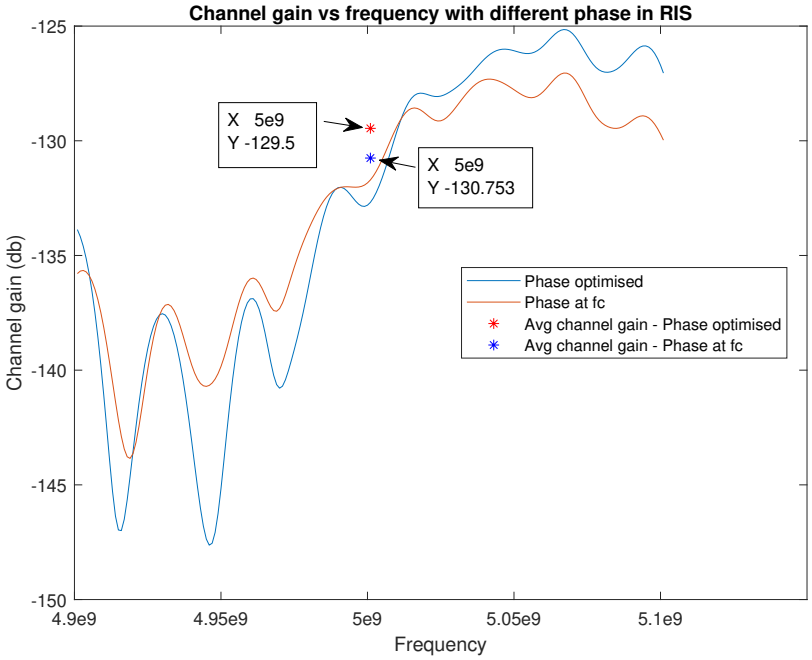

Figure 5.13: Channel gain between BS1 - RIS1 - UE1

The red and blue asterisks in Figure 5.13 show the average received power using the optimized phase information and the phase information obtained at the center frequency. The channel gain observed in Figure 5.13 clearly shows an improvement when using the optimized phase values. Although the difference in channel gain is not significant, it does not mean that optimization for phase is unnecessary. Figure 5.13 only represents the channel between BS at position 1, RIS at position 1, and UE at position 1. We believe that optimization is necessary when we consider the entire simulation environment.

It is important to mention that unconstrained optimization heavily depends on the starting position we provide for the input variable vector. We have verified the effect of starting positions on the above optimizations by randomizing input vectors and evaluating the results. From our observation, we conclude that using the phase information obtained at the center frequency as the starting position for optimization yields the same optimum solution but is quicker than any other starting position.

Chapter 6

RIS Performance in Heavily Shadowed Environments

In Section 5.3, we have explained in great detail the trade-offs in received power for different selections of BSs and RISs. Our observation indicated strong LOS in many of the UE positions from the predefined path in Figure 4.1. After optimization, the observation matrix revealed that the direct link is picked almost 50% of the time compared to the RIS-assisted link, even with a considerable gain in RIS (for example, 26dB). Although this is satisfactory, we wish not to have such high gains in the power amplifier due to practical issues that arise with it. Moreover, the presence of the RISs is better justified when significant shadowing is present in the environment. This has been our motivation to change the positions of BSs, RISs, and UE trajectory, and they can be seen in Figure 6.1

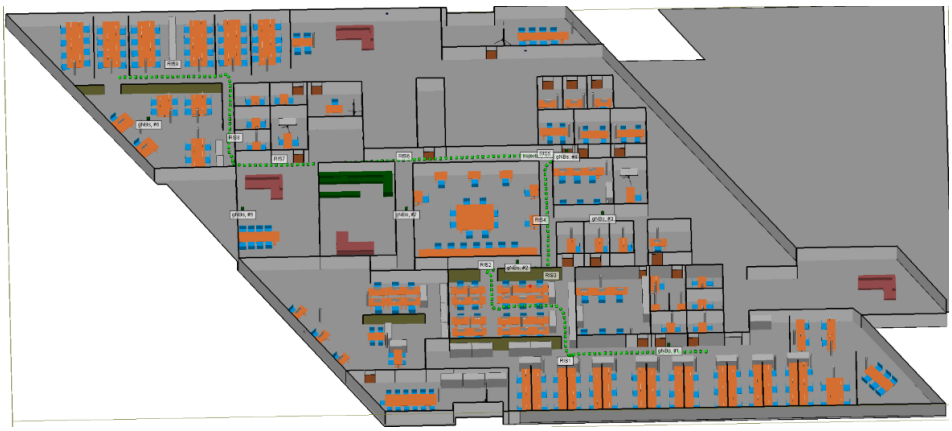

Figure 6.1: NLOS - simulation environment with more shadowing

In this environment, we have moved the UE trajectory through corridors. We can provide some conclusions about this after the results are presented.

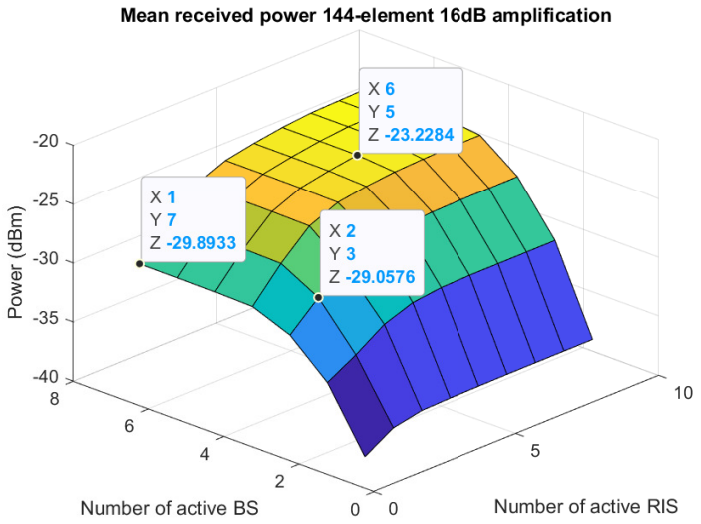

Figure 6.2: RIS performance in heavily shadowed environment

Figure 6.2 is the surface plot of the mean received power performance of the communication system in this heavily shadowed environment with an input power of 30 dBm. Notably, the validity of this result holds in the narrowband system. As shown, each RIS has 144 elements, and the power amplification is 16 dB. It is important to mention that Figure 6.2 is still evaluated in the narrowband case.

Based on Figure 6.2, Figure 5.9, and Figure 5.11, one can conclude that:

- Deploying three RISs and two BSs can achieve the same performance as deploying seven BSs and one RIS.
- Only five BSs and six RISs are needed to achieve the upper limit of the mean received power.
- The RISs are more power efficient in heavily shadowed environments.
- RISs are more beneficial for the communication system in heavily shadowed communication environments.

Chapter 7

Conclusion and Future work

7.1 Conclusion

From the surface plots generated in Section 5.3.3, we provide graphical data representing the trade-offs in received power when we change the number of BSs and RISs. We can clearly observe that having more RIS with very few BSs does not lead to a significant increase in received power, allowing us to conclude that we need at least three active BSs deployed in the scenario to see any acceptable improvement in minimum power offered by using a RIS. Furthermore, we need more RIS in the environment to take advantage of the increased number of BSs. Moreover, we observe plateau regions in the surface plots indicating the maximum performance of the system can be achieved without utilizing all BSs and RISs. This plateau region can be reached quickly, in other words, with less number of BSs and RISs when there is more shadowing in the environment. It is also important to note that we have mathematical data available to corroborate the fact that RIS becomes more relevant to deployment when the shadowing in the environment is predominant.

Using a RIS with 24 dB amplification ensures an improvement of 18dB in the minimum power for 5 BSs and 4 RIS, and 11dB improvement can be observed in the mean power for 12 BSs and 4 RIS. We also conclude that using RISs equipped with 30dB power amplifiers allows the UE to circumvent a direct link. In other words, using a maximum of 30dB power amplifier allows the RIS-assisted link to outperform the direct link. The QoS figure in the outage optimization indicates at least three BSs are needed to ensure a stable QoS. We conclude that a 5% outage is a better choice when considering power efficiency and QoS together, meaning designing the system to drop 5% of UEs is a good trade-off in our scenario. From the preset locations of BSs, we conclude that increasing the number of BSs beyond a certain extent does not guarantee increasing mean power. There is an upper bound on maximum mean power that is achieved at twelve BSs. There is also an upper bound for the minimum received power which can be seen in the case of five BSs. Although these numbers are restricted to our scenario, we can say in general that increasing the number of BSs is not beneficial to the system as interference becomes predominant. We have observed that the upper bounds obtained when only using direct links can be breached by deploying RISs. This can also be seen in the surface plots provided in the RIS-assisted link.

After discussing in great detail about optimization, we show that many RIS-related problems can be formulated as linear programming problems and solved using optimization. We also conclude that using MILP is a faster and more practical solution to arrive at the optimum selection of BSs and RISs within the environment. As the solution from the MILP solver is a subset of the exhaustive search, we need not carry out the exhaustive search for RIS-assisted link and outage scenarios. It is necessary to remember that the optimal solution is better than any random selection only when the entire system is being considered. Random choices might have more power received compared to the optimal solution at certain positions, but the mean value will always be better for the optimum solution. The configuration of mean and minimum power can take multiple optimum values based on constraints given, i.e., there might be more than one optimum configuration possible and can be seen in the upper boundary figures. In the mean and minimum power configurations, we can observe a degradation in mean power if we wish to have increased minimum power and vice versa. The method given for this solution allows the operator to configure their networks based on their system requirements.

From various iterations, we have observed that using phase compensation values obtained at center frequency results in the faster computation of optimal phase for RIS elements. We were not able to conclude on the gain from using optimal phase in the RIS when compared to using phase obtained at center frequency, as it requires around 70,000 optimization iterations from the method we have discussed. This was left as an extension for this master thesis.

7.2 Future work

The thesis work we presented can be extended in many directions. Here, we list some future work that can be done:

- Ray tracing based investigation of RIS performance in the high-frequency spectrum such as 28GHz.
- More accurate ray tracing simulations with the help of high-performance computers and LiDAR.
- RIS in this thesis is assumed to achieve perfect beamforming to the impinging signals and to the UE, which indicates the RIS can perform continuous phase shifts to the signals. Achieving quantized phase shifts is more feasible for RIS implementation. The performance of RIS-assisted communication systems with discrete phase shifts remains unanswered.
- The power amplification of every RIS is assumed to be identical, which is not smart enough. How to control the power amplification of each RIS smartly, and how much is the performance loss?
- Utilizing the reciprocity of the propagation channel to obtain the downlink channel from a RIS to a UE. In real life, estimating the channel at a RIS is still an open challenge.

- The optimization of the phase shifts at each RIS is proved to be critical in a wideband communication system. However, the RIS performance in a wideband communication system is not studied in this thesis.

References

[1] H. Tataria, M. Shafi, A. F. Molisch, M. Dohler, H. Sjöland and F. Tufvesson, "6G Wireless Systems: Vision, Requirements, Challenges, Insights, and Opportunities," in Proceedings of the IEEE, vol. 109, no. 7, pp. 1166-1199, July 2021, doi: 10.1109/JPROC.2021.3061701.

[2] X. Cai, X. Cheng, and F. Tufvesson, "Toward 6G with Terahertz Communications: Understanding the Propagation Channels," in IEEE Communications Magazine, (accepted), preprint available at https://doi.org/10.1109/MCOM.001.2200386.

[3] N. Suneetha and P. Satyanarayana, "Intelligent Channel Estimation in Millimeter Wave Massive MIMO Communication System Using Hybrid Deep Learning with Heuristic Improvement," in International Journal of Communication Systems, vol. 36, no. 5, March 2023, doi: https://doi-org.ludwig.lub.lu.se/10.1002/dac.5400.

[4] F. Adachi, R. Takahashi, H. Matsuo, S. Xia, C. Ge and Q. Chen, "On Design Concept of Cellular Distributed MU-MIMO for Ultra-dense RAN," 2022 27th Asia Pacific Conference on Communications (APCC), Jeju Island, Korea, Republic of, 2022, pp. 266-271, doi: 10.1109/APCC55198.2022.9943686.

[5] J. Vieira and E. G. Larsson, "Reciprocity Calibration of Distributed Massive MIMO Access Points for Coherent Operation," 2021 IEEE 32nd Annual International Symposium on Personal, Indoor and Mobile Radio Communications (PIMRC), Helsinki, Finland, 2021, pp. 783-787, doi: 10.1109/PIMRC50174.2021.9569495.

[6] T. Y. Elganimi and K. M. Rabie, "Multi-IRS-aided Millimeter-wave Massive MIMO with Energy-Efficient Hybrid Precoding Schemes," 2022 IEEE Wireless Communications and Networking Conference (WCNC), Austin, TX, USA, 2022, pp. 1075-1080, doi: 10.1109/WCNC51071.2022.9771604.

[7] E. Basar, M. Di Renzo, J. De Rosny, M. Debbah, M. -S. Alouini and R. Zhang, "Wireless Communications Through Reconfigurable Intelligent Surfaces," in IEEE Access, vol. 7, pp. 116753-116773, 2019, doi: 10.1109/ACCESS.2019.2935192.

[8] X. Yuan, Y. -J. A. Zhang, Y. Shi, W. Yan and H. Liu, "Reconfigurable-Intelligent-Surface Empowered Wireless Communications: Challenges and Opportunities," in IEEE Wireless Communications, vol. 28, no. 2, pp. 136-143, April 2021, doi: 10.1109/MWC.001.2000256.

[9] H. Zhang, B. Di, L. Song, and Z. Han, "Reconfigurable Intelligent Surface-Empowered 6G," Berlin, Germany: Springer, 2021.

[10] B. J. B. Deutschmann, T. Wilding, E. G. Larsson and K. Witrisal, "Location-based Initial Access for Wireless Power Transfer with Physically Large Arrays," 2022 IEEE International Conference on Communications Workshops (ICC Workshops), Seoul, Korea, Republic of, 2022, pp. 127-132, doi: 10.1109/ICCWorkshops53468.2022.9814679.

[11] H. Alidoustaghdam, Y. Miao and A. Kokkeler, "Integrating TDD Communication and Radar Sensing in Co-Located Planar Array: A Genetic Algorithm Enabled Aperture Design," 2022 2nd IEEE International Symposium on Joint Communications & Sensing (JC&S), Seefeld, Austria, 2022, pp. 1-6, doi: 10.1109/JCS54387.2022.9743500.

[12] Z. Wei et al., "5G PRS-Based Sensing: A Sensing Reference Signal Approach for Joint Sensing and Communication System," in IEEE Transactions on Vehicular Technology, vol. 72, no. 3, pp. 3250-3263, March 2023, doi: 10.1109/TVT.2022.3215159.

[13] A. Behravan et al., "Positioning and Sensing in 6G: Gaps, Challenges, and Opportunities," in IEEE Vehicular Technology Magazine, vol. 18, no. 1, pp. 40-48, March 2023, doi: 10.1109/MVT.2022.3219999.

[14] M. Di Renzo et al., “Smart Radio Environments Empowered by Reconfigurable AI Meta-Surfaces: An Idea Whose Time Has Come,” in EURASIP Journal on Wireless Communications and Networking, vol.2019, no.1, pp. 1–20, May 2019, doi: https://doi.org/10.48550/arXiv.1903.08925.

[15] Z. Yun and M. F. Iskander, "Ray Tracing for Radio Propagation Modeling: Principles and Applications," in IEEE Access, vol. 3, pp. 1089-1100, 2015, doi: 10.1109/ACCESS.2015.2453991.

[16] M. Hassan-Ali and K. Pahlavan, "Site-specific Wideband and Narrowband Modeling of Indoor Radio Channel Using Ray-tracing," Ninth IEEE International Symposium on Personal, Indoor and Mobile Radio Communications (Cat. No.98TH8361), Boston, MA, USA, 1998, pp. 65-68 vol.1, doi: 10.1109/PIMRC.1998.733512.

[17] H. Lu, D. Zhao, Y. Wang, C. Kong and W. Chen, "Joint Power Control and Passive Beamforming in Reconfigurable Intelligent Surface Assisted User-Centric Networks," in IEEE Transactions on Communications, vol. 70, no. 7, pp. 4852-4866, July 2022, doi: 10.1109/TCOMM.2022.3174071.

[18] Q. Wu and R. Zhang, "Towards Smart and Reconfigurable Environment: Intelligent Reflecting Surface Aided Wireless Network," in IEEE Communications Magazine, vol. 58, no. 1, pp. 106-112, January 2020, doi: 10.1109/MCOM.001.1900107.

[19] Z. Zhang et al., "Active RIS vs. Passive RIS: Which will Prevail in 6G?," in IEEE Transactions on Communications, vol. 71, no. 3, pp. 1707-1725, March 2023, doi: 10.1109/TCOMM.2022.3231893.

Appendix A

Some extra material

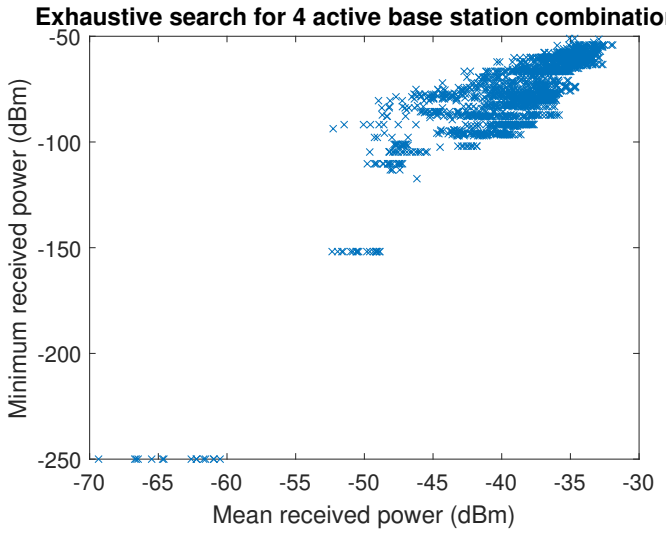

Figure A.1: Exhaustive search for optimum subsets of 4 BSs

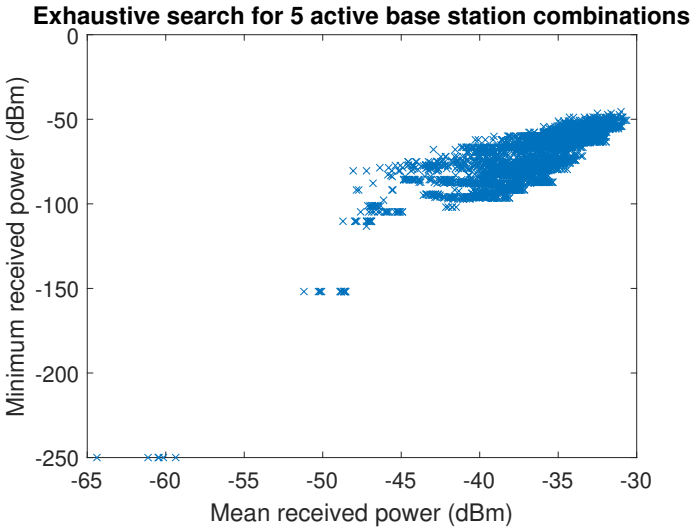

Figure A.2: Exhaustive search for optimum subsets of 5 BSs

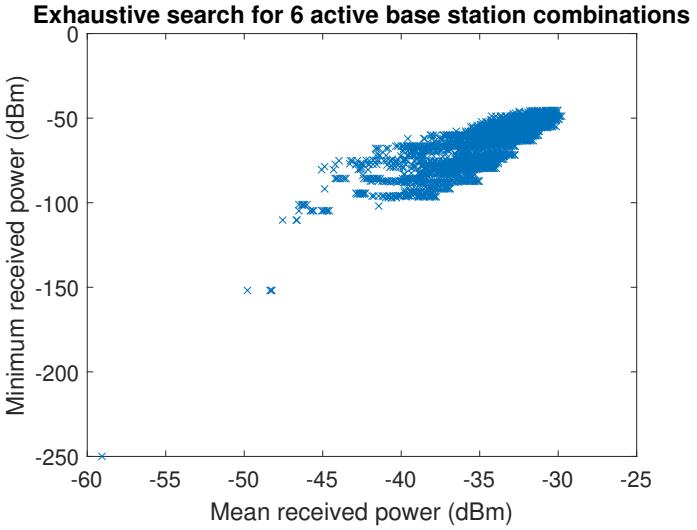

Figure A.3: Exhaustive search for optimum subsets of 6 BSs

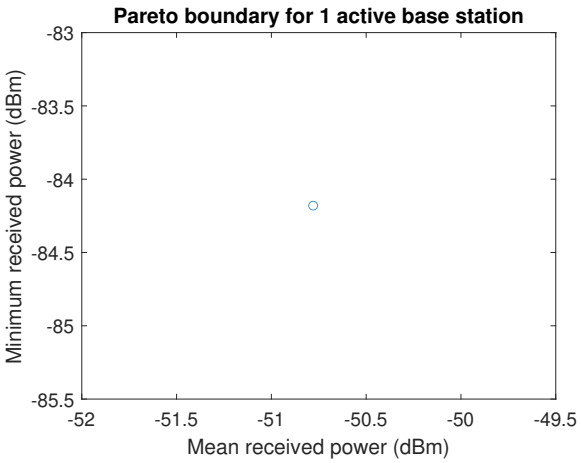

Figure A.4: Pareto boundary for 1 active BS

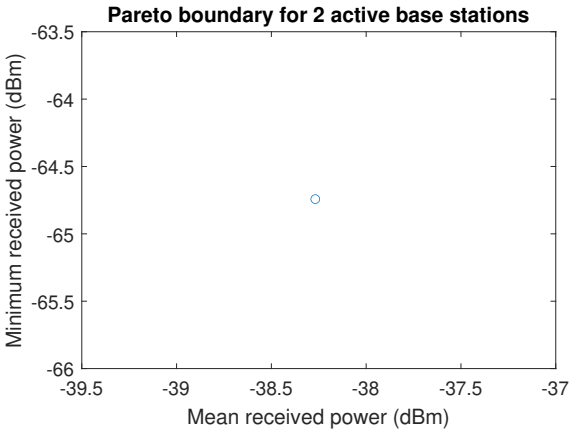

Figure A.5: Pareto boundary for 2 active BSs

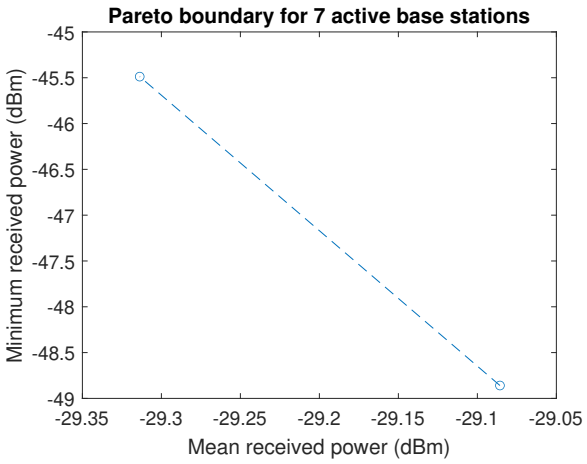

Figure A.6: Pareto boundary for 7 active BSs

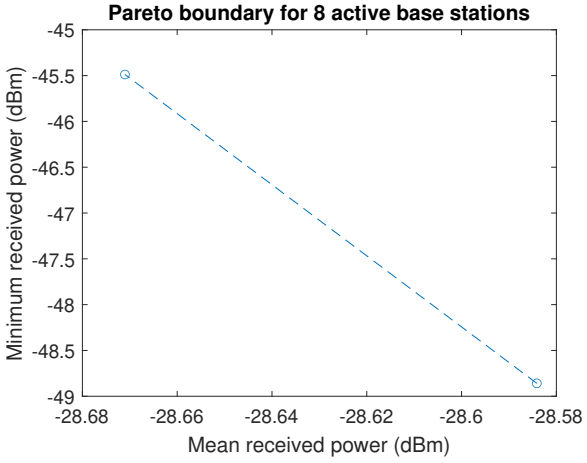

Figure A.7: Pareto boundary for 8 active BSs

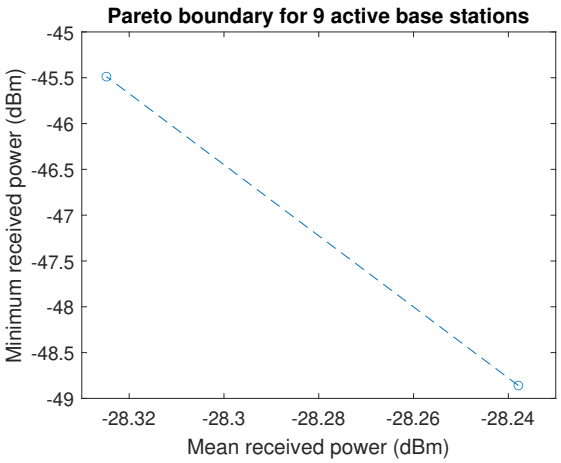

Figure A.8: Pareto boundary for 9 active BSs

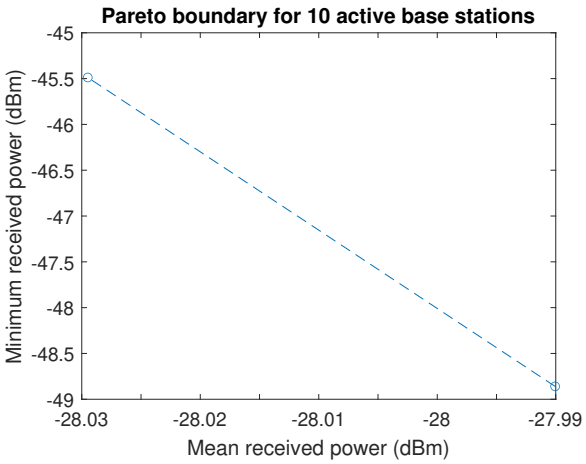

Figure A.9: Pareto boundary for 10 active BSs

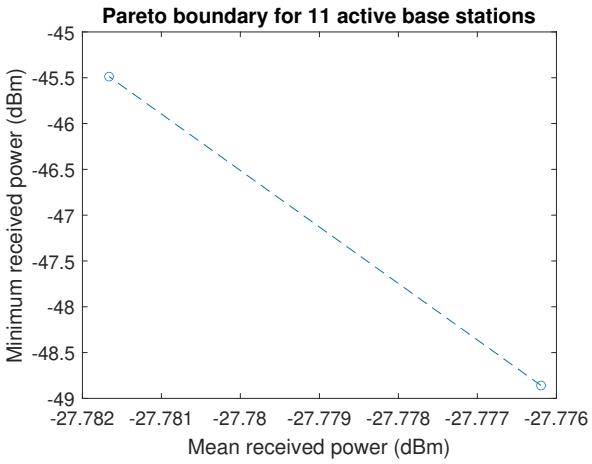

Figure A.10: Pareto boundary for 11 active BSs

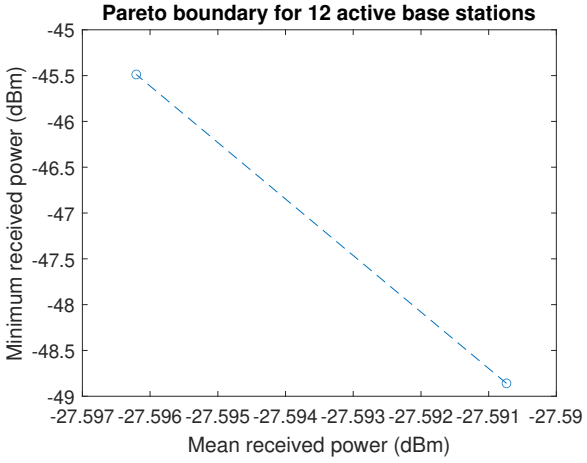

Figure A.11: Pareto boundary for 12 active BSs

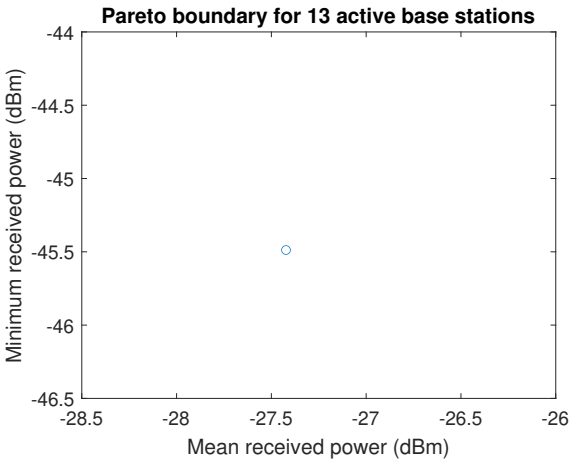

Figure A.12: Pareto boundary for 13 active BSs

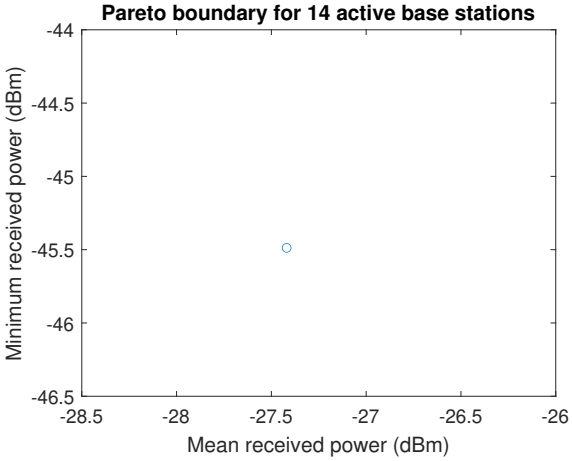

Figure A.13: Pareto boundary for 14 active BSs

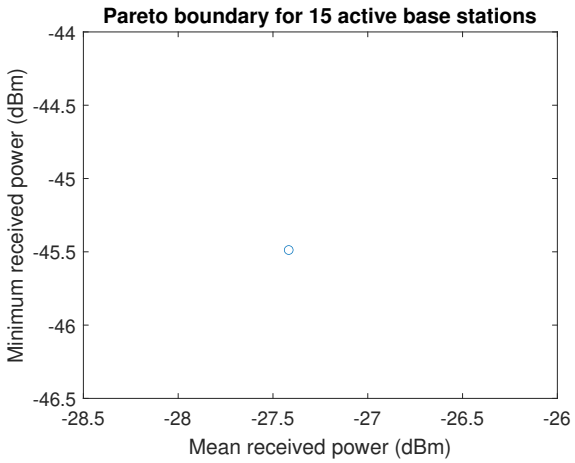

Figure A.14: Pareto boundary for 15 active BSs

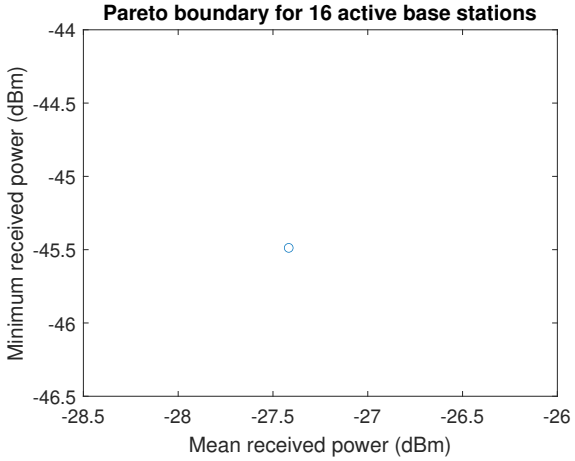

Figure A.15: Pareto boundary for 16 active BSs

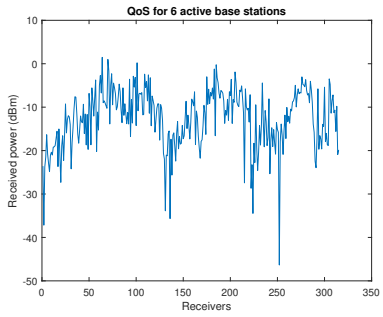

(a) QoS with 6 active BSs

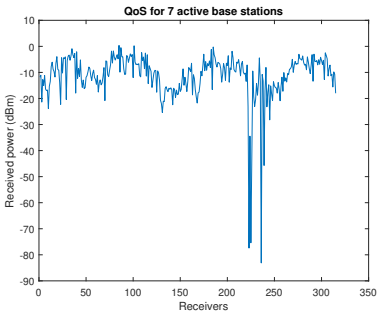

(b) QoS with 7 active BSs

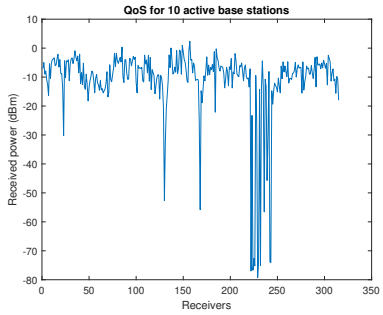

(c) QoS with 10 active BSs

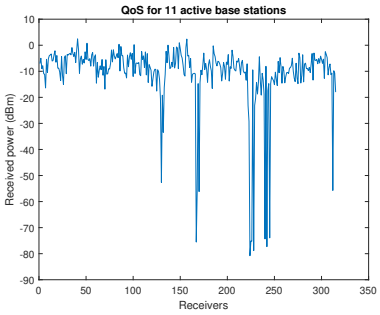

(d) QoS with 11 active BSs

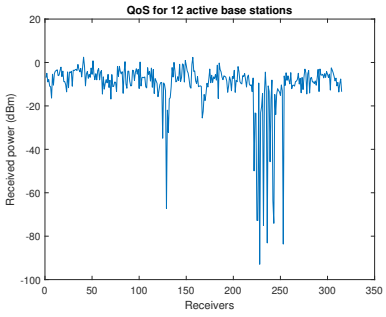

(e) QoS with 12 active BSs

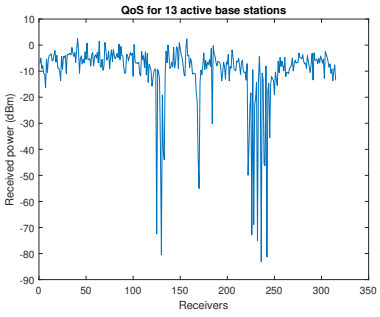

(f) QoS with 13 active BSs

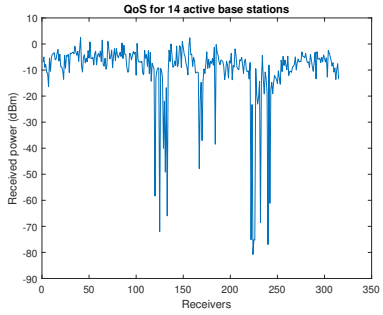

(g) QoS with 14 active BSs

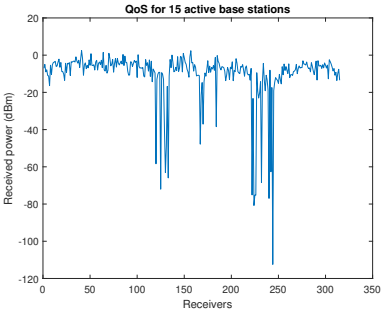

(h) QoS with 15 active BSs

Figure A.16: QoS with 5% outage probability

Printed by Tryckeriet i E-huset, Lund 2023

LUND
UNIVERSITY

Series of Master's theses
Department of Electrical and Information Technology
LU/LTH-EIT 2023-930
http://www.eit.lth.se